CHAPTER 4

RADIATION BY FLUCTUATING-VOLUME (MONOPOLE) SOURCES

As discussed in Chapter 3, motions of boundaries that cause fluctuations of fluid volume are the most efficient radiators of sound. The basic fluctuating-volume source is a small, pulsating spherical surface, called a *monopole*, which radiates sound uniformly in all directions. Monopoles are defined as spherical sources whose dimensions are small compared to an acoustic wavelength. Larger fluctuating-volume sources can be considered to be composed of many monopoles, and their pressure fields can be found by superposition of monopole fields.

The approach taken in the present chapter is to develop the equations for a uniformly pulsating sphere of arbitrary size, and then to obtain the properties of monopoles by taking the limit as size becomes very small. The equations derived for pulsating spheres are then applied to air bubbles pulsating in liquids, and those for monopoles used to calculate pressure fields of linear arrays, pistons and hull openings. Brief consideration is also given to several approaches for the calculation of radiation fields of arbitrary vibrating surfaces. The final section is an overview of hull radiation. Two other important practical examples of fluctuating-volume sources, namely plate bending waves and cavitation, are treated in later chapters.

4.1 Uniformly Pulsating Spherical Source

As an introduction to monopoles, it is useful to consider radiation from uniformly pulsating spherical sources of arbitrary size. Monopole radiation is then simply the limit as size approaches zero. The methodology used is similar to that employed in most fundamental radiation problems. An expression for the acoustic particle velocity in a fluid medium is matched to the normal surface vibratory velocity of a solid boundary, and the acoustic pressure is then found from the acoustic impedance.

Consider a spherical cavity having a mean radius a_o experiencing a uniform, small harmonic fluctuation of its volume. This volume fluctuation causes a rate-of-change of fluid in the medium, i.e., a mass flux, Q, which can be expressed by

$$Q(t) \equiv \rho_o \dot{V}(t) = Q_o \cos \omega t = RP\left[Q_o e^{i\omega t}\right] . \tag{4.1}$$

By assuming that the relative change of volume of the sphere is small, one can write the flux in terms of the product of the area and radial velocity of the surface,

$$Q(t) \doteq \rho_o \left(4\pi a_o^2\right)\dot{a} = \rho_o S_o u \quad . \tag{4.2}$$

It follows that the instantaneous surface velocity can be expressed by

$$\underline{u} = u_o e^{i\omega t} = \frac{Q_o}{4\pi a_o^2 \rho_o} e^{i\omega t} . \tag{4.3}$$

Since the fluid is everywhere in contact with the vibrating surface, the acoustic particle speed, $v'(a_o)$, must equal the surface vibratory speed, u. With this relation, the acoustic pressure at the surface of the sphere can be calculated by multiplying the vibratory speed, u, by the specific acoustic impedance evaluated at the surface. From Eqs. 2.78 and 2.79, it follows that

$$\underline{p}'(a_o) = \underline{z}_a(a_o)\underline{v}'(a_o) = \rho_o c_o \frac{(ka_o)^2 + i(ka_o)}{1 + (ka_o)^2} \underline{u}$$

$$= \frac{\omega Q_o}{4\pi a_o} \frac{1}{\sqrt{1 + (ka_o)^2}} e^{i(\omega t + \theta_a)} , \tag{4.4}$$

where θ_a is the phase angle between the pressure and the velocity on the surface of the sphere, as defined by Eq. 2.80, and as given by

$$\theta_a \equiv \tan^{-1}\left(\frac{1}{ka_o}\right) . \tag{4.5}$$

It follows that the pressure at distance r from the center of the sphere is

$$\underline{p}'(r) = \frac{a_o}{r} \underline{p}'(a_o) e^{-ik(r - a_o)}$$

$$= \frac{\omega Q_o}{4\pi r} \frac{e^{i(\theta_a + ka_o)}}{\sqrt{1 + (ka_o)^2}} e^{i(\omega t - kr)} . \tag{4.6}$$

This expression has a form typical of that for the radiated acoustic pressure of many different types of sources. The first term is independent of the relative size and shape of the source and includes the first-power dependence on distance from the origin typical of spherical spreading. The second term involves ka_o and expresses something about the size and/or shape of the specific radiator, in this case the size relative to an acoustic wavelength. The final, exponential, term represents a propagating harmonic disturbance.

Intensity and Power

The intensity and power of a spherical source can be calculated from the pressure, using expressions derived in Section 2.4. The intensity is

$$I = \frac{\overline{p'^2}}{\rho_o c_o} = \frac{\omega^2 Q_o^2}{32\pi^2 r^2 \rho_o c_o} \cdot \frac{1}{1 + (ka_o)^2} , \tag{4.7}$$

and the total radiated power is

$$W_{ac} = \int_S I\,dS = 4\pi r^2 I = \frac{\omega^2 Q_o^2}{8\pi\rho_o c_o} \cdot \frac{1}{1 + (ka_o)^2} . \tag{4.8}$$

Radiation Impedance

As indicated in Section 3.1, acoustic power can also be expressed as the product of the radiation resistance and the mean-square surface velocity. From Eqs. 3.3, 4.3 and 4.8 it follows that the specific radiation resistance is given by

$$\sigma_r \equiv \frac{R_r}{\rho_o c_o S_o} = \frac{W_{ac}}{\rho_o c_o S_o \overline{u^2}} = \frac{(ka_o)^2}{1 + (ka_o)^2} . \tag{4.9}$$

As shown in Fig. 4.1, this factor is proportional to the square of ka_o for small values and approaches unity in the limit of large ka_o. The specific radiation reactance is given by the imaginary term in Eq. 4.4 as

$$\sigma_x \equiv \frac{X_r}{\rho_o c_o S_o} = \frac{ka_o}{1 + (ka_o)^2} , \tag{4.10}$$

which function is also plotted in Fig. 4.1.

The total radiation impedance is the ratio of the force exerted on the surface of the uniformly vibrating sphere to the surface velocity. It is simply the surface area multiplied by the specific

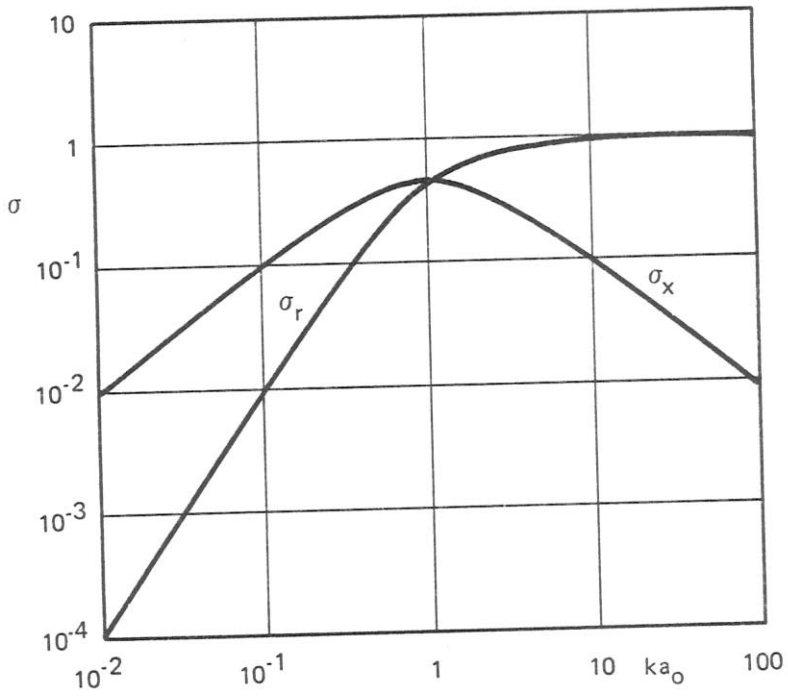

Fig. 4.1. Specific Radiation Impedance for Uniformly Pulsating Sphere

acoustic impedance evaluated at the surface,

$$\underline{Z}_r = S_o \underline{z}_a(a) = \rho_o c_o S_o \frac{(ka_o)^2 + i(ka_o)}{1 + (ka_o)^2} . \tag{4.11}$$

Radiation Efficiency

The radiation efficiency, defined by Eqs. 1.4 and 3.4, is

$$\eta_{rad} = \frac{R_r}{\sqrt{R_r^2 + X_r^2}} = \frac{\sigma_r}{\sqrt{\sigma_r^2 + \sigma_x^2}} = \frac{ka_o}{\sqrt{1 + (ka_o)^2}} . \tag{4.12}$$

As shown in Fig. 4.2, the radiation efficiency is a linear function of ka_o for small spheres and approaches unity for large ones. The first-power dependence of the radiation efficiency on ka_o is a characteristic of small, fluctuating-volume sources, as discussed in Chapter 3.

Entrained Mass

The reactive component of the radiation impedance is that of the mass of the fluid participating in the motion, i.e., the mass entrained by the motion of the spherical surface. The *entrained mass* can be calculated by dividing the reactance by the angular frequency, ω, giving

$$m_e = \frac{X_r}{\omega} = \frac{\rho_o S_o a_o}{1 + (ka_o)^2} = \frac{3}{1 + (ka_o)^2}\left(\frac{4}{3}\pi a_o^3 \rho_o\right) = \frac{3\rho_o V_o}{1 + (ka_o)^2} . \tag{4.13}$$

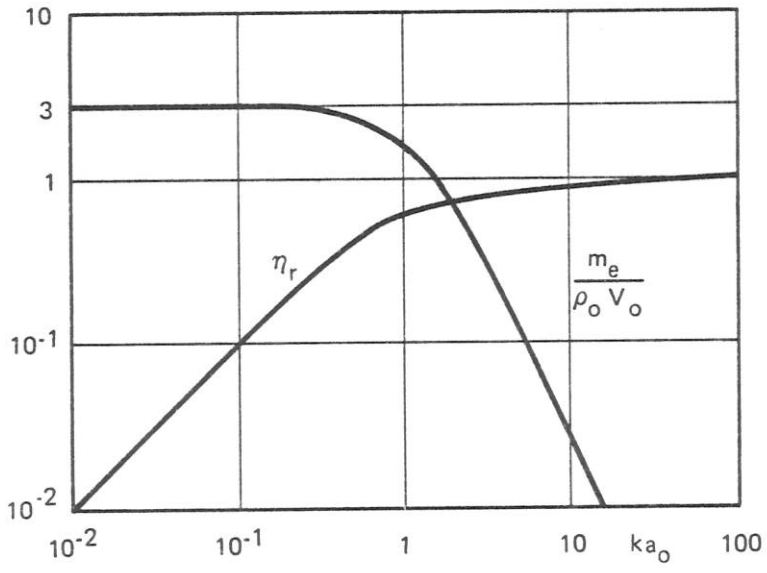

Fig. 4.2. Radiation Efficiency and Relative Entrained Mass for Spherical Sources

Thus, for small values of ka_o the entrained mass is three times the mass of the displaced fluid, while for large values it approaches zero. The relative entrained mass is also plotted in Fig. 4.2.

4.2 Monopole Radiation

The general expressions presented in the previous section for spherical sources of arbitrary size are directly usable whenever a spherical radiator can be treated as pulsating uniformly, such as in the case of pulsating bubbles, treated in Section 4.3. However, it is more useful to consider spherical sources that are small compared to an acoustic wavelength. Monopoles are characterized by $ka << 1$. With this stipulation, the phase angle θ_a between the pressure and the velocity at the surface becomes

$$\theta_a = tan^{-1}\left(\frac{1}{ka_o}\right) \doteq \frac{\pi}{2} - ka_o \ , \tag{4.14}$$

and the second term in Eq. 4.6 reduces to i. The radiated pressure at distance r from the center of the source is then

$$\underline{p}'(r) = i\,\frac{\omega Q_o}{4\pi r}\,e^{i(\omega t - kr)} \ . \tag{4.15}$$

The intensity is given by

$$I(r) = \frac{\overline{p^2}}{\rho_o c_o} = \frac{\omega^2 Q_o^2}{32\pi^2 r^2 \rho_o c_o} \ , \tag{4.16}$$

and the total power radiated is

$$W_{ac} = \frac{\omega^2 Q_o^2}{8\pi\rho_o c_o} \ . \tag{4.17}$$

The specific radiation resistance and reactance given by Eqs. 4.9 and 4.10 reduce to

$$\sigma_r = (ka_o)^2 \tag{4.18}$$

and

$$\sigma_x = ka_o \ , \tag{4.18}$$

from which it follows that the radiation efficiency for a monopole is

$$\eta_{rad} = ka_o \ . \tag{4.20}$$

From Eq. 4.13, the mass entrained by a monopole is three times the mass of the displaced fluid.

These same results could have been derived by starting with Eq. 3.28 for the acoustic pressure associated with volume acceleration. Assuming an harmonic oscillation, Eq. 3.28 leads to

$$p'(r) = \frac{\rho_o \ddot{V}}{4\pi r} = \frac{\dot{Q}(t')}{4\pi r} = \frac{i\omega Q_o}{4\pi r} e^{i\omega(t - r/c_o)} , \tag{4.21}$$

which result is equivalent to that of Eq. 4.15. The expressions for intensity and power follow directly. The specific radiation resistance is then calculated from Eq. 3.3, giving

$$\sigma_r = \frac{W_{ac}}{\rho_o c_o S_o \overline{u^2}} = (ka_o)^2 . \tag{4.22}$$

Since the radiation efficiency of a monopole was derived for a general spherical multipole of zero order, Eq. 3.22, and shown to be equal to ka_o, it follows that the reactance ratio is

$$\sigma_x = \frac{\sigma_r}{\eta_{rad}} = \frac{(ka_o)^2}{ka_o} = ka_o = \frac{\omega a_o}{c_o} , \tag{4.23}$$

leading to the conclusion that the reactance is equal to three times that of the mass of the displaced fluid,

$$X_r = \rho_o c_o S_o \sigma_x = \rho_o \omega 4\pi a_o^3 = 3\omega \rho_o V_o , \tag{4.24}$$

in full agreement with the result obtained by letting ka_o approach zero in Eq. 4.13.

4.3 Sounds from Gas Bubbles in Liquids

It is not uncommon to find gas bubbles present in the ocean, in streams and in pipe flows. Minnaert (1933) concluded that the almost musical sounds of running water are caused by air bubbles oscillating at their natural frequencies and radiating as monopoles. Sounds are also radiated when bubbles flow into regions of varying hydrodynamic pressure. Examples of this are bubbles entrained near the bow of a ship when acted on by the pressure field of that ship and when passing through its propeller, and bubbles flowing through a constriction in a pipe or around a pipe bend. Sound is also generated when bubbles form, collapse, divide or coalesce. The sounds radiated by these phenomena can be estimated by using a differential equation for bubble wall motion to find the volume acceleration and then using Eq. 4.21 to calculate the sound pressure. While changes of shape invariably accompany volume pulsations, Strasberg (1956) has shown that any sound radiated by such changes is negligible and that valid estimates of sound radiation can be made by considering only volume effects.

Linear Bubble Pulsations

Volume pulsations of a gas bubble in a liquid can be treated as a mass-spring system in which the mass of entrained liquid provides inertia, and adiabatic compression of the gas acts as a spring. Resistance to the motion is caused by liquid viscosity, thermal losses in the gas and radiation of sound energy. Differential equations for bubble motions can be derived by equating the sum of the forces acting at the bubble surface to the rate-of-change of momentum of the entrained liquid. Such equations usually include surface-tension forces and several non-linear terms. However, a linear second-order differential equation can be used to analyze relatively small pulsations of gas-filled bubbles. Strasberg (1956) has written this equation in terms of the bubble volume, V, as

$$m_e \ddot{V} + R\dot{V} + K(V(t) - V_o) = S_o^2(p_o - p(t)) \ , \tag{4.25}$$

where m_e is the entrained mass, as given by Eq. 4.13, K is the spring constant of the compressed gas inside the bubble and R is a coefficient of resistance. Subscripts zero refer to equilibrium values of the static pressure, p, and the bubble volume, V. The spring constant can be derived from thermodynamic relations for a nearly spherical volume,

$$K \equiv - \frac{dF}{da} = - S \frac{dp}{da} \doteq - S_o^2 \frac{dp}{dV} \ . \tag{4.26}$$

For an adiabatic process, for which pV^{γ} = constant, the spring constant is given by

$$K = \gamma S_o^2 \frac{p_o}{V_o} = \frac{3\gamma S_o p_o}{a_o} \ , \tag{4.27}$$

where γ is the ratio of the specific heats of the gas inside the bubble.

Second-order linear differential equations of the form of Eq. 4.25 are quite common in mechanics as well as in other branches of physics, and their solutions are well known. The complete solution is composed of two parts: that of the homogeneous equation for which the applied force is set equal to zero, and a solution having the same form as the applied force. The solution of the homogeneous equation describes the motion when the system is acted on by a transient disturbance and allowed to respond freely. The nature of the solution depends on the relative amount of damping. Bubbles are generally lightly damped and the applicable solution is that of a damped oscillation, of the form

$$\underline{V} = V_o + \underline{A} e^{-\alpha t} e^{i\omega_o t} \ , \tag{4.28}$$

where $\underline{A}$ is the amplitude of the motion as determined by initial values of the volume and its time derivative, and α is a *dissipation coefficient* given by

$$\alpha = \frac{R}{2m_e} \ . \tag{4.29}$$

The ratio of the resistance coefficient to the inertial reactance of the entrained mass at the frequency of oscillation is called the *loss factor*, η, and is related to the dissipation coefficient by

$$\eta \equiv \frac{R}{\omega_o m_e} = 2 \frac{\alpha}{\omega_o} \ . \tag{4.30}$$

In most instances, the loss factor is less than unity, and Eq. 4.28 then represents an exponentially damped oscillation having a rate of decay that is slow compared to the period of oscillation, as depicted in Fig. 4.3. The period between maxima is simply the reciprocal of the frequency,

$$T_o = \frac{1}{f_o} = \frac{2\pi}{\omega_o} \ . \tag{4.31}$$

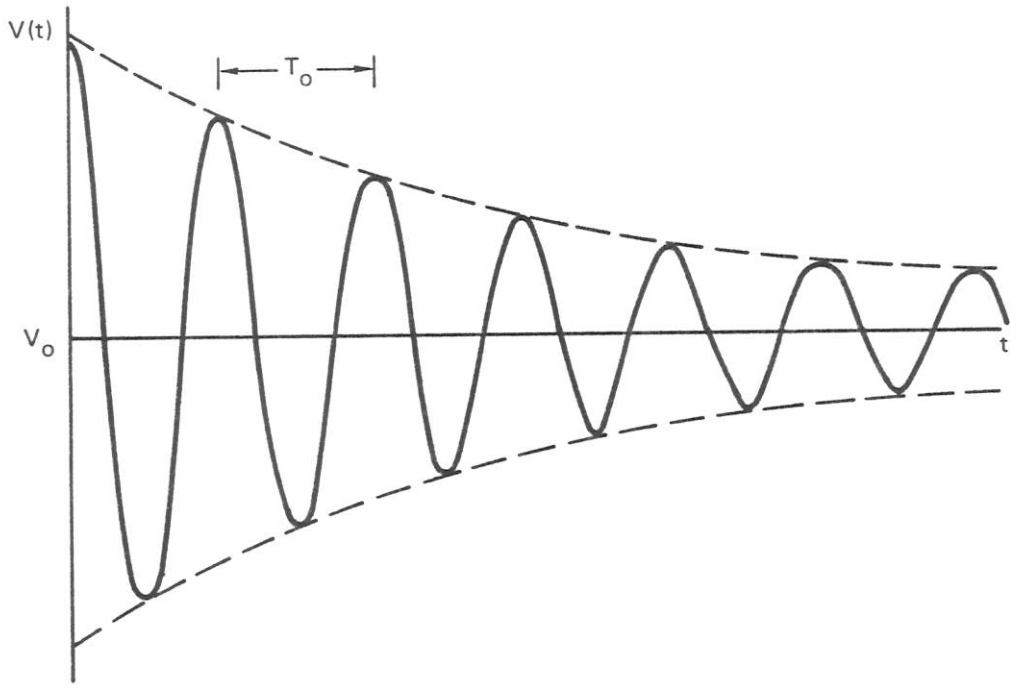

Fig. 4.3. Damped Oscillation of a Gas Bubble

and the relative decay in one period is the *logarithmic decrement*, δ, given by

$$\delta \equiv ln \frac{1}{e^{-\alpha T_o}} = \alpha T_o = \frac{2\pi\alpha}{\omega_o} = \pi\eta \ . \tag{4.32}$$

Since the mechanical energy of a vibrating system is proportional to the square of the amplitude of its vibration, it follows that for a lightly damped system the relative energy lost in one vibrational period is 2δ, or $2\pi\eta$.

The complex amplitude, $\underline{A}$, of the motion is an involved function of the initial volume displacement, $\Delta V(0)$, and the initial volume velocity, $\dot{V}(0)$. Its magnitude is given by

$$A = \Delta V(0) \sqrt{1 + \frac{\eta}{\omega_o} \frac{\dot{V}(0)}{\Delta V(0)} + \left(\frac{1}{\omega_o} \frac{\dot{V}(0)}{\Delta V(0)} \right)^2} \ , \tag{4.33}$$

and its phase angle, ϕ, by

$$\phi = - \tan^{-1} \left(\frac{\eta}{2} + \frac{\dot{V}(0)}{\omega_o \Delta V(0)} \right) . \tag{4.34}$$

In most situations the initial velocity is small; hence the magnitude A equals the initial displacement, $\Delta V(0)$, and the phase angle ϕ reduces to $- \eta/2$.

Frequency of Bubble Oscillation

An expression for the resonance frequencies of gas bubbles in liquids was first derived by Minnaert (1933). He assumed that damping is negligible and that the bubble diameter is small compared to the wavelength. Thus, ignoring damping,

$$\ddot{V} = -\omega_o^2 (V - V_o) , \tag{4.35}$$

and the homogeneous form of Eq. 4.28 becomes

$$(-\omega_o^2 m_e + K)(V - V_o) = 0 , \tag{4.36}$$

from which

$$f_o \equiv \frac{\omega_o}{2\pi} \doteq \frac{1}{2\pi}\sqrt{\frac{K}{m_e}} = \frac{1}{2\pi}\sqrt{\frac{3\gamma S_o p_o}{3\rho_o V_o a_o}} = \frac{1}{2\pi a_o}\sqrt{\frac{3\gamma p_o}{\rho_o}} . \tag{4.37}$$

Minnaert's experiments with gas bubbles in water appeared to confirm this expression and to justify his assumptions. When damping is included, the resonance frequency is modified slightly, the more complete expression being

$$f_o = \frac{1}{2\pi}\sqrt{\frac{K}{m_e} - \alpha^2} \doteq \frac{1}{2\pi}\sqrt{\frac{K}{m_e}}\left(1 - \frac{\eta^2}{8}\right) . \tag{4.38}$$

Thus, the effect of damping on the resonance frequency is less than 1% if $\eta < 0.3$, which condition is invariably satisfied in low-viscosity liquids such as water.

In deriving Eq. 4.37, Minnaert assumed that the entrained mass equals three times the displaced mass, which follows from Eq. 4.13 provided $(ka_o)^2 << 1$. Combining Eqs. 4.13 and 4.37,

$$ka_o = \frac{\omega_o a_o}{c_o} = \sqrt{\frac{3\gamma p_o}{\rho_o c_o^2}}\sqrt{1 + (ka_o)^2} . \tag{4.39}$$

For air bubbles in water at pressures up to several hundred atmospheres, this reduces to

$$ka_o \doteq 0.0136\sqrt{P_A} , \tag{4.40}$$

where P_A is the static pressure in atmospheres. The assumption is therefore verified for static pressures up to 100 atm. Under this condition, Eq. 4.37 yields

$$f_o \doteq \frac{3.28}{a_o}\sqrt{P_A} \quad Hz \tag{4.41}$$

for the resonance frequency of an air bubble in water. Thus, an air bubble having a radius of 1 mm in water at 1 atm. would have a resonance frequency of about 3.3 kHz.

Equations 4.37 and 4.41 for the natural frequencies of bubbles are accurate for bubbles that are neither too small nor too large. If bubbles are smaller than about 3×10^{-3} cm in diameter, surface tension and viscosity raise the frequency, while bubbles larger than 1 cm tend to take

shapes so far removed from spherical that the assumptions made in deriving Eqs. 4.13 and 4.27 are not valid. Strasberg (1953) has shown that the resonance frequency of a prolate spheroid having a 2:1 ratio of its axes is 2% higher than that calculated by Eq. 4.37. The effects of nearby boundaries on bubble pulsations, which are more serious, are beyond the scope of the present volume.

Damping Mechanisms

As indicated above, damping has only a secondary effect on bubble resonance frequencies, but it controls the rate of decay of bubble pulsations set into motion by transient disturbances. A number of investigators have made theoretical calculations and experimental measurements of bubble damping. In a survey of this subject, Devin (1959) listed three dominant mechanisms:

1) sound radiation,
2) thermal losses in the gas, and
3) viscous losses in the liquid.

Of these, only sound radiation is independent of bubble size. Both thermal and viscous losses increase with decreasing bubble size.

For a bubble containing an ideal gas pulsating in an ideal, lossless liquid, the only loss mechanism would be the radiation of sound itself. The loss factor, η, of the vibratory motion would then equal the radiation efficiency of a vibrating sphere, as given by Eq. 4.12. Combining with Eq. 4.39, the loss factor would be given by

$$\eta \doteq \eta_{rad} = \frac{ka_o}{\sqrt{1 + (ka_o)^2}} = \sqrt{\frac{3\gamma p_o}{\rho_o c_o^2}} , \tag{4.42}$$

which for air bubbles in water is

$$\eta \doteq \eta_{rad} = 0.0136 \sqrt{P_A} . \tag{4.43}$$

Devin and others have shown that, for most air bubbles in water at atmospheric pressure, thermal damping equals or exceeds radiation damping, becoming as much as an order of magnitude greater for bubbles having diameters of less than 10^{-2} cm. Viscous losses are not important in water, but are usually dominant in oil. Measurements of damping factors made by different investigators are not in complete agreement. Figure 4.4 presents approximate values, based on the summary of results published by Devin (1959).

Sound Radiation

The sound radiated by a gas bubble excited into resonant vibration can be calculated using equations developed in Sections 4.1 and 4.2. Most of these equations are expressed in terms of the mass flux, Q, which equals the volume velocity, $\dot{V}$, multiplied by the fluid density. Taking the time derivative of the bubble volume, as given in Eq. 4.28, and assuming the loss factor, η, to be small compared to unity, it follows that

$$\underline{Q}(t') \equiv \rho_o \underline{\dot{V}}(t') = i\omega_o \rho_o A e^{i(\phi + \eta/2)} e^{-(\eta/2)\omega_o t'} e^{i\omega_o t'} , \tag{4.44}$$

where t' is retarded time as defined by Eq. 2.6. In most cases the transient disturbance can be assumed to have created a difference, ΔV, between the initial volume and the equilibrium value,

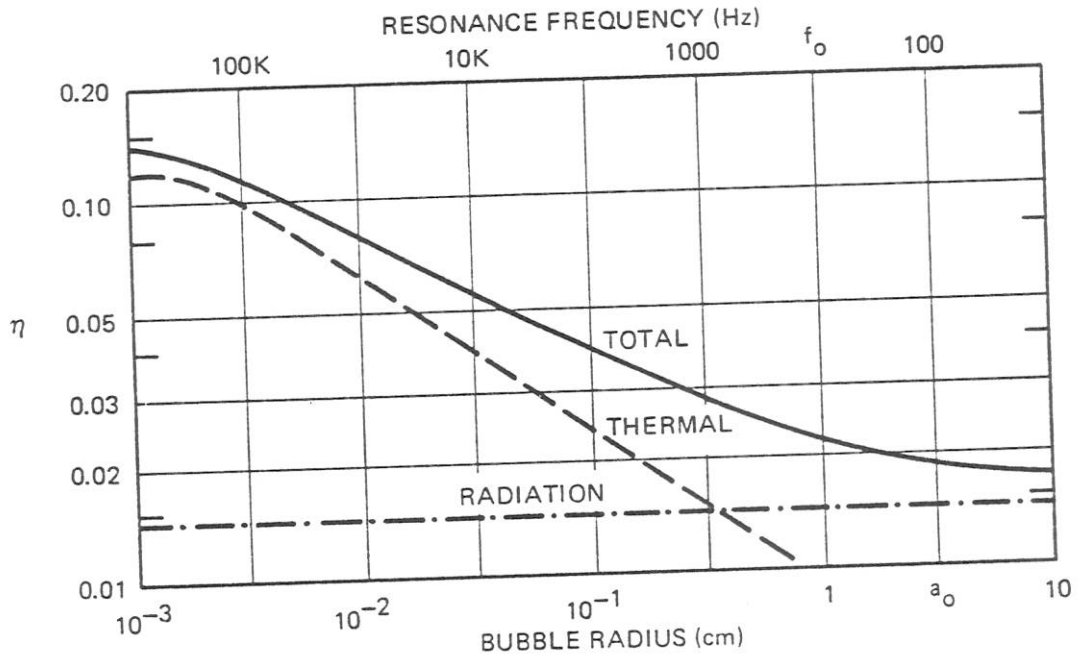

Fig. 4.4. Damping of Resonant Air Bubbles at Atmospheric Pressure, after Devin (1959)

and $\dot{V}(0)$ can be assumed to be zero. In these cases, Eq. 4.44 for the mass flux reduces to

$$\underline{Q}(t') = i\omega_o \rho_o \Delta V \, e^{-(\eta/2)\omega_o t'} \, e^{i\omega_o t'} \, . \tag{4.45}$$

It follows from Eq. 4.15 that the acoustic pressure at distance r is given by

$$\underline{p}'(r,t) = i \frac{\omega Q_o(t')}{4\pi r} e^{i(\omega t - kr)} \doteq - \frac{\rho_o \omega_o^2 \Delta V}{4\pi r} e^{-(\eta/2)(\omega_o t - k_o r)} e^{i(\omega_o t - k_o r)} \, , \tag{4.46}$$

where the minus sign implies that an oversize bubble will initially contract, thereby creating a rarefaction. The amplitude of the acoustic pressure can be expressed as a function of the static pressure, bubble dimensions and ratio of specific heats by using Eq. 4.37 for the resonant frequency. The resultant expression,

$$\left| \underline{p}'(r,t) \right| = \frac{\gamma p_o}{r/a_o} \frac{\Delta V}{V_o} e^{-(\eta/2)(\omega_o t - k_o r)} \, , \tag{4.47}$$

shows that, other factors being equal, the peak pressure increases linearly with bubble diameter.

It is of interest to calculate the total energy radiated by a bubble given an initial volume displacement. From Eqs. 4.17 and 4.45, the instantaneous power is

$$W_{ac} = \frac{\omega^2 Q_o^2}{8\pi \rho_o c_o} = \frac{\rho_o \omega_o^4 (\Delta V)^2}{8\pi c_o} e^{-\eta \omega_o t'} \, . \tag{4.48}$$

Integrating from the time of the disturbance,

$$E_{ac} = \int_0^\infty W_{ac}\,dt' = \frac{\rho_o \omega_o^3 (\Delta V)^2}{8\pi c_o \eta} . \tag{4.49}$$

Using Eq. 4.37 for the resonance frequency and utilizing Eq. 4.20 for the radiation efficiency, the total energy radiated during the entire decay period is

$$E_{ac} = \frac{\gamma p_o (\Delta V)^2}{2V_o} \frac{\eta_{rad}}{\eta} = \frac{1}{2} \Delta p \Delta V \frac{\eta_{rad}}{\eta} , \tag{4.50}$$

where Δp is the magnitude of pressure change associated with volume change ΔV for an adiabatic expansion of a constant amount of gas.

The above equations have been derived for a constant-mass gas bubble and apply to such cases as a bubble set into oscillation by passage through a pressure jump, as in a pump, or to a bubble acted on by a pressure pulse. Strasberg (1956) has shown that the result is essentially the same when a bubble is formed at a nozzle, Δp being the excess pressure of the gas supply forming the bubbles, and ΔV being the final volume of each bubble. Sound is also emitted when bubbles split or coalesce. In this case, the pressure difference causing the volume change is the difference between the surface tension pressures of the two sizes of bubbles.

Most practical examples of bubble noise involve many bubbles. Since the sounds add incoherently, the acoustic power is simply N times the radiated energy per bubble, where N is the number of bubbles experiencing the pressure jump or volume change each second. Thus, the sound radiated by a gas jet in water should be primarily controlled by the flow rate and not influenced significantly by the size of the orifice. This result has been verified by Mühle and Heckl (1971), who measured the sound when gas jets discharge into still water. However, measurements by Gavigan, Watson and King (1974) in a water tunnel have shown that when gas discharges into a moving turbulent flow the orifice size is a critical parameter. Apparently bubble breakup and collapse can be a dominant noise-generating mechanism in a turbulent flow.

4.4 Sounds from Splashes

Splashes associated with the impact of water droplets on the ocean surface are a major source of underwater noise. The droplets are generally created by breaking waves, but are also caused by rain and by the breaking of surface ship bow waves. While numerous photographs of the resultant spatter have been published, very little attention has been given in the literature to underwater noise aspects. The only thorough study of this subject known to the author is that of Franz (1959).

Franz's Measurements

Franz measured the underwater noise produced by the impacts of single drops as well as that from sprays of droplets. He found that two distinct noise mechanisms account for the sound, and that both radiate with cosine directional patterns typical of near-surface sources. A sharp pulse is radiated by the actual impact of a water drop on the surface, and this is followed by sounds emitted by bubble volume pulsations. Impact sounds are proportional to the kinetic energy and cube of the Mach number of the impacting body, but bubble sounds are quite erratic and do not

vary consistently with droplet size or velocity. Franz was able to separate the two types of sounds and to measure their spectra individually.

The spectra radiated by the impact phase of splashing water droplets were found to cover a wide frequency band and to vary consistently with drop size and impact speed. Figure 4.5 summarizes Franz's results for this type of sound. It can be seen that a broad peak is centered at a dimensionless frequency close to unity, decreasing at a rate approaching 5 dB/octave at the higher frequencies. For drops of a given size, the sound radiated increases by 13 to 17 dB for a factor of 2 increase of the impact velocity.

Sounds from bubble pulsations were found to be more nearly sinusoidal, producing spectra with relatively sharp peaks, generally between 500 Hz and 10 kHz. Franz found that bubble sounds usually dominate in the octave for which they are strongest, with impact sounds controlling the spectrum at the other frequencies, as illustrated in Fig. 4.6.

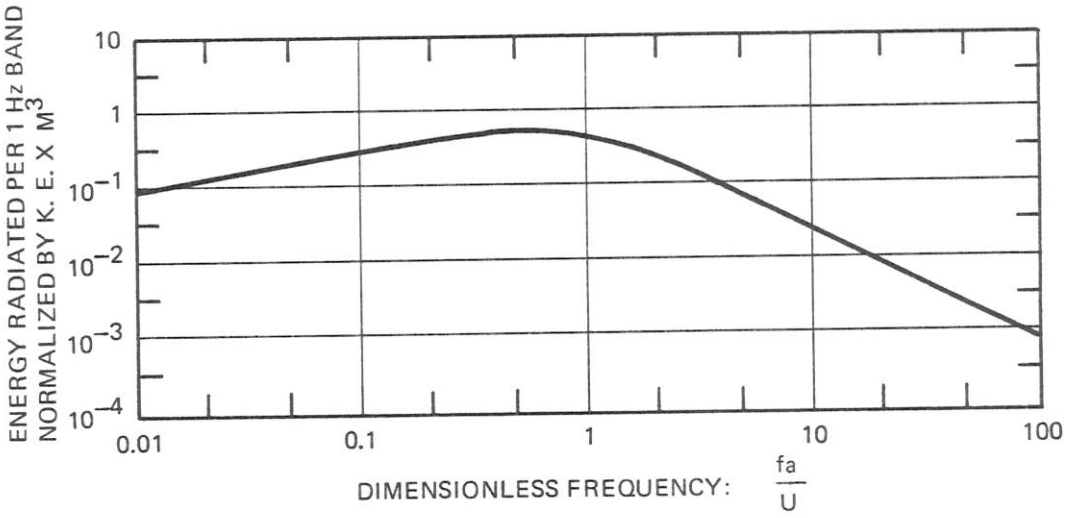

Fig. 4.5. Spectra of Sounds From Surface Impacts, as measured by Franz (1959)

Wind-Generated Ambient Sea Noise

Splash noise from breaking waves is a major source of underwater ambient noise, generally dominating measured spectra above 300 Hz and sometimes being dominant to as low as 20 Hz. Noise levels measured during World War II, mostly above 500 Hz, were almost invariably controlled by the degree of agitation of the sea surface as described either by wind speed or sea state. The famous summary curves published by Knudsen, Alford and Emling (1944, 1948) and reproduced in Fig. 4.7 have a constant - 5 dB/octave slope extending from 100 Hz to over 30 kHz. However, measurements made following the end of WWII revealed that levels below about 200 Hz are often independent of sea state and that extrapolation of the Knudsen curves below 500 Hz is erroneous. It was found that the spectral shape of the sea agitation contribution to ambient noise is quite similar to that reported by Franz for splash noise (as depicted in Fig. 4.5) with the peak frequency occurring between 300 and 600 Hz.

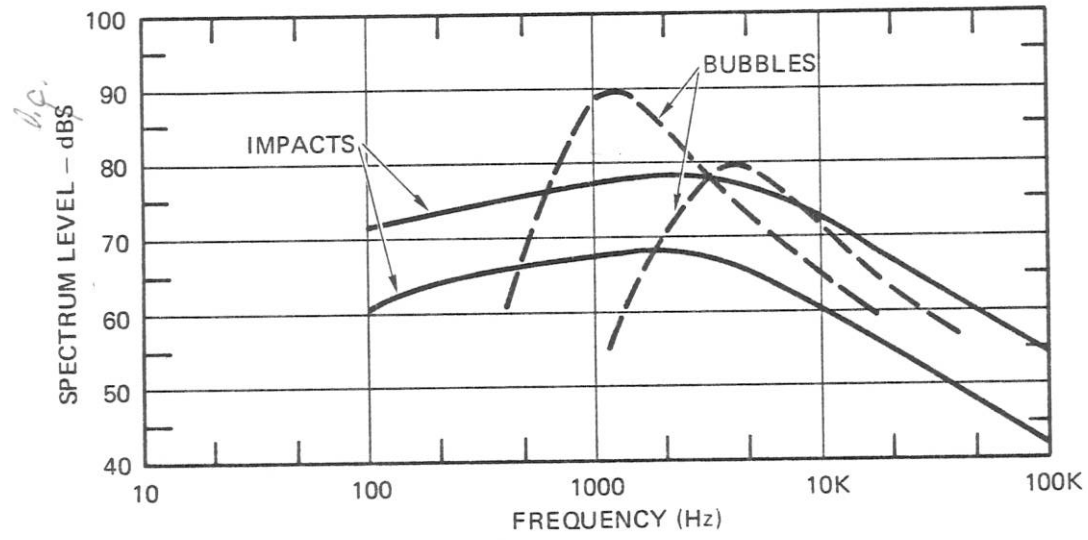

Fig. 4.6. Sounds From Splashes, after Franz (1959)

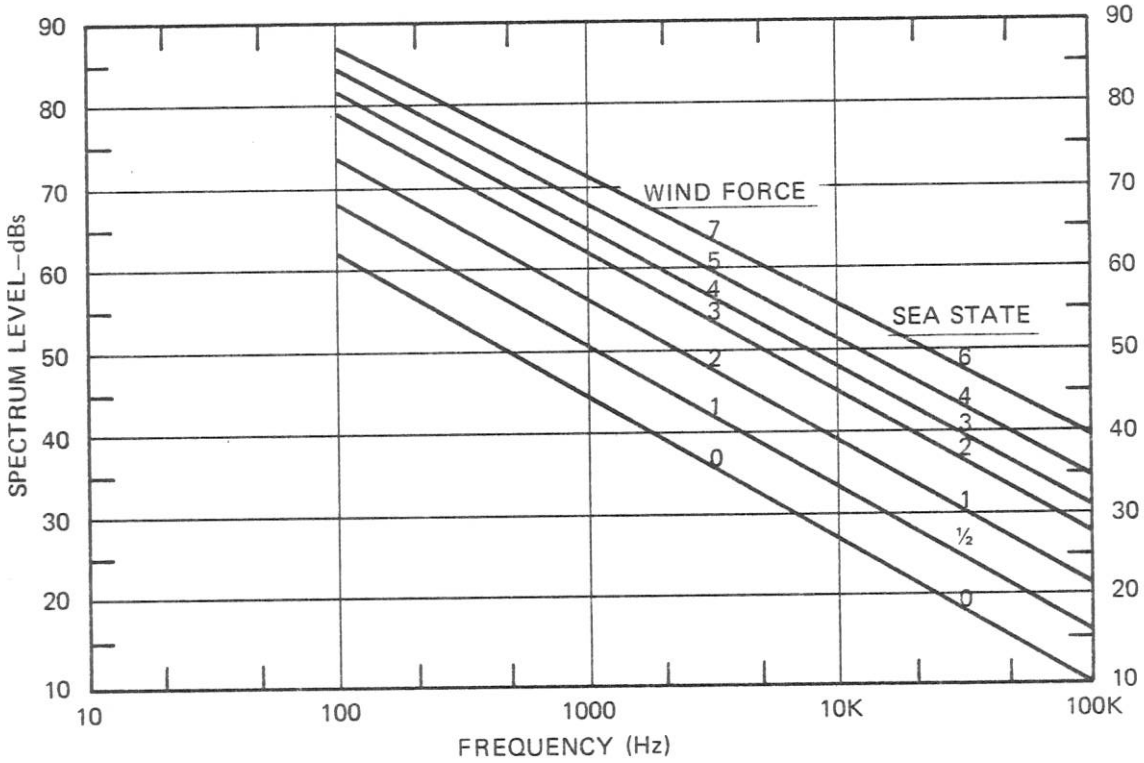

Fig. 4.7. Knudsen Average Ambient Spectra (1944)

In a comprehensive summary paper, Wenz (1962) attributed the wind-independent noise at low frequencies to distant shipping, which source is discussed in Chapter 8. Measurements made at low frequencies in remote regions free of shipping show spectra that are practically flat from 20 to 500 Hz, decreasing above this frequency at a rate of about 5 dB/octave. Figure 4.8 summarizes a number of these modern measurements of wind-generated deep-water ambient noise. As indicated in this figure, deep-water levels above 1 kHz are somewhat lower than those reported for the same wind speed by Knudsen et al. On the other hand, Piggott (1964) and others have reported shallow-water levels higher than the Knudsen values, and a trend to lower levels in deeper water was also found by Perrone (1970). Apparently the curves developed from WWII data apply to medium water depths of the order of 100 fathoms. In any case, the important feature shown by the curves in Fig. 4.8 is the peaks at about 400 Hz with slight decreases below this frequency. This results in levels as much as 15 to 25 dB below Knudsen extrapolated values for frequencies below 100 Hz.

Rain Noise

The spectra generated by breaking waves are typical of what would be expected from Franz's results for droplet impact speeds of the order of only a few meters per second. Raindrops fall at higher speeds and so produce spectra with higher peak frequencies as well as higher levels. Figure 4.9 shows several typical rain-generated ambient noise spectra, as measured by Heindsman et al (1955) and Bom (1969) for several rain rates. At 10 kHz the levels are as much as 20 to 30 dB higher than those typical of breaking waves.

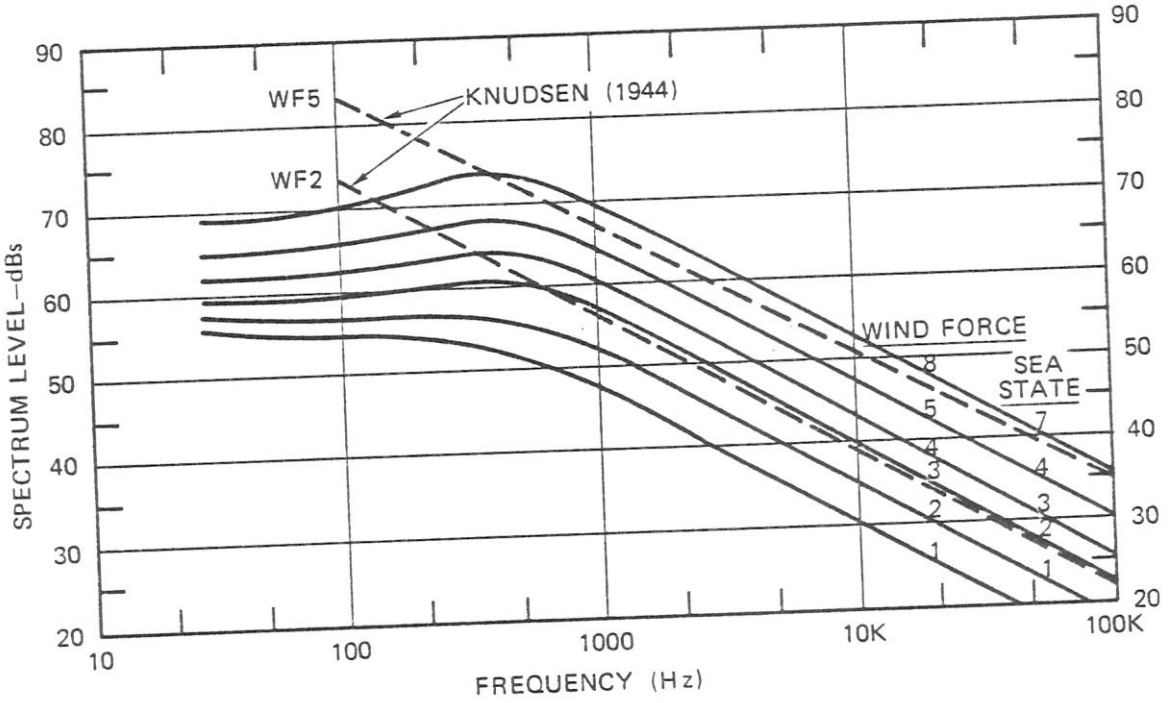

Fig. 4.8. Wind-Generated, Deep-Water Ambient Noise Spectra

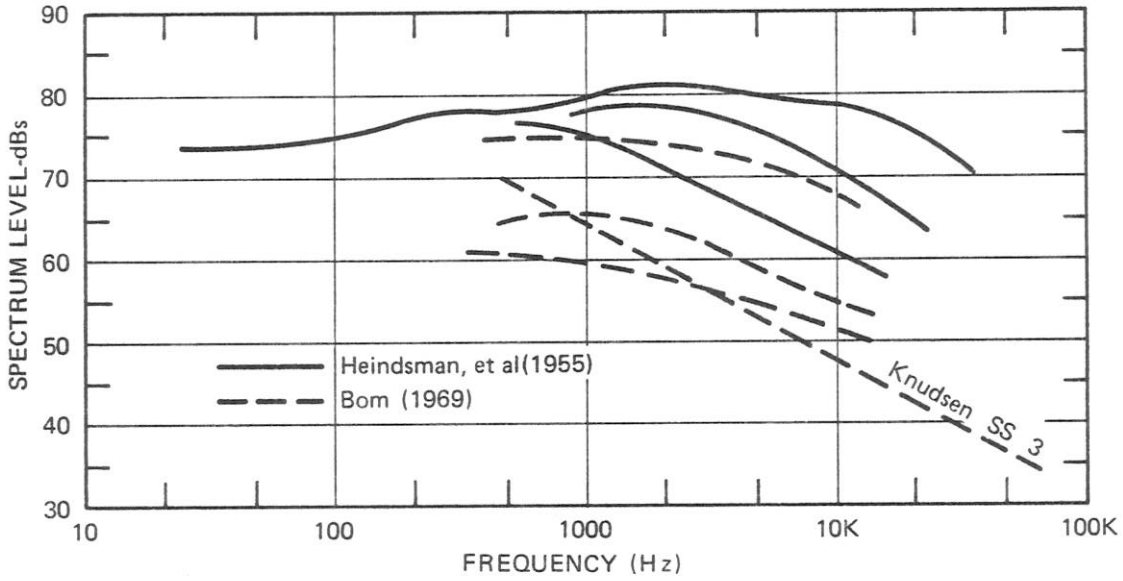

Fig. 4.9. Examples of Measured Rain Noise in Shallow Water

4.5 Radiation by Two Equal Monopoles

Many practical fluctuating-volume noise sources have dimensions that are large compared to a wavelength. The sound fields resulting from such sources can in principle be calculated by dividing their surfaces into a large number of small sources and then summing all the individual sound fields, being careful to retain phase information. Such calculations are often quite laborious and usually require high-powered computers. The topic of the present section is radiation from two equal monopoles separated by an arbitrary distance, which is the simplest example illustrative of the calculation for a large radiator.

General Equation for Pressure Field

Consider two equal monopoles radiating at exactly the same frequency and separated by distance d, as depicted in Fig. 4.10. Their midpoint is taken as origin. The field point, P, at which the pressure is to be calculated is located at distance r from the origin that may or may not be large compared to their separation. The x axis is taken to be perpendicular to their connecting line, and θ is the angle of the field point relative to this axis. The distances r_1 and r_2 of the individual sources from the field point are given by

$$r_1^2 = r^2 \cos^2\theta + \left(r\sin\theta - \frac{d}{2}\right)^2$$

$$= r^2 + \left(\frac{d}{2}\right)^2 - rd\sin\theta \quad , \tag{4.51}$$

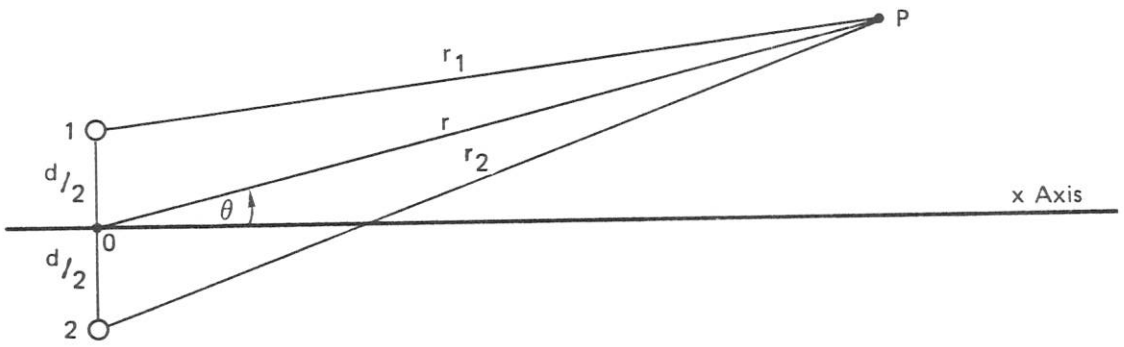

Fig. 4.10. Geometric Representation of Two Monopoles

and

$$r_2^2 = r^2 \cos^2\theta + \left(r \sin\theta + \frac{d}{2}\right)^2$$

$$= r^2 + \left(\frac{d}{2}\right)^2 + rd \sin\theta \quad . \tag{4.52}$$

It is useful to express these distances in terms of the *rms distance*, $\bar{r}$, defined by

$$\bar{r} \equiv \sqrt{\overline{r^2}} = \sqrt{\frac{r_1^2 + r_2^2}{2}} = \sqrt{r^2 + \left(\frac{d}{2}\right)^2} \quad . \tag{4.53}$$

and a dimensionless parameter, β, defined by

$$\beta \equiv \frac{rd}{r_1^2 + r_2^2} \sin\theta = \frac{rd}{2\bar{r}^2} \sin\theta \quad . \tag{4.54}$$

The expressions for the distances r_1 and r_2 can then be written

$$r_1 = \bar{r}\sqrt{1 - \frac{rd}{\bar{r}^2} \sin\theta} = \bar{r}\sqrt{1 - 2\beta} \quad , \tag{4.55}$$

and

$$r_2 = \bar{r}\sqrt{1 + \frac{rd}{\bar{r}^2} \sin\theta} = \bar{r}\sqrt{1 + 2\beta} \quad . \tag{4.56}$$

The acoustic pressure at the field point is simply the sum of the individual monopole pressure fields as given by Eq. 4.15, namely

$$\underline{p}' = \frac{i\omega Q_o}{4\pi r_1} e^{i(\omega t - kr_1)} + \frac{i\omega Q_o}{4\pi r_2} e^{i(\omega t - kr_2 - \psi)} , \tag{4.57}$$

where ψ is the phase angle of the second source relative to the first. It is useful to calculate this resultant pressure field in terms of that which would exist at distance $\bar{r}$ from a single source located at the origin and radiating with the average phase angle. Defining such a reference pressure by

$$\underline{p}'_o \equiv \frac{i\omega Q_o}{4\pi \bar{r}} e^{i(\omega t - k\bar{r} - \psi/2)} , \tag{4.58}$$

Eq. 4.57 for the pressure field of the two sources becomes

$$\underline{p}' = \underline{p}'_o \left[\frac{e^{ik\bar{r}(1 - \sqrt{1 - 2\beta})}}{\sqrt{1 - 2\beta}} e^{i(\psi/2)} + \frac{e^{ik\bar{r}(1 - \sqrt{1 + 2\beta})}}{\sqrt{1 + 2\beta}} e^{-i(\psi/2)} \right] . \tag{4.59}$$

This result is valid throughout the pressure field. Except in the immediate vicinity of each source, the parameter β is less than 0.2. With this condition, the square roots in Eq. 4.59 can each be expanded as a power series. Retaining only the linear terms, one obtains an approximate expression for the pressure,

$$\underline{p}' \doteq \underline{p}'_o \left[\frac{e^{i(\beta k\bar{r} + (\psi/2))}}{1 - \beta} + \frac{e^{-i(\beta k\bar{r} + (\psi/2))}}{1 + \beta} \right] , \tag{4.60}$$

which is valid throughout most of the field.

Far-Field Pressure Pattern

Most often interest is limited to the far field that exists at distances large compared to the separation between the sources. At these long ranges all distances can be assumed to be equal, and the parameter β is small compared to unity. Substituting for β from Eq. 4.54, Eq. 4.60 reduces to

$$\underline{p}' \doteq \underline{p}'_o \left[e^{i((kd/2) \sin\theta + (\psi/2))} + e^{-i((kd/2) \sin\theta + (\psi/2))} \right] . \tag{4.61}$$

From Eq. 1.58, the sum of the two exponential terms can be replaced by a trigonometric function, leading to

$$\underline{p}' = 2\underline{p}'_o \cos\left(\frac{kd}{2} \sin\theta + \frac{\psi}{2} \right) , \tag{4.62}$$

and to the alternative form

$$\underline{p}' = \underline{p}'_o \frac{\sin(kd \sin\theta + \psi)}{\sin\left(\frac{kd}{2} \sin\theta + \frac{\psi}{2} \right)} . \tag{4.63}$$

The pressure patterns described by these two equivalent expressions have maxima whenever the argument of the cosine is zero or a multiple of π, that for zero being called the *principal maximum* and the others being secondary maxima. The angle, θ_o, of the principal maximum is related to the phase shift by

$$\theta_o = -\sin^{-1}\frac{\psi}{kd} . \tag{4.64}$$

Expressing the phase difference, ψ, in terms of this angle, Eq. 4.62 for the pressure field can be written

$$\underline{p}' = 2\underline{p}'_o \cos\frac{kd}{2}(\sin\theta - \sin\theta_o) . \tag{4.65}$$

Directivity Function

When calculating or measuring the far-field radiated pressure field of any large source, it is customary to express the result in terms of the pressure in the direction of the principal maximum multiplied by the normalized pressure pattern, or *directivity function*, $D(\theta)$, defined by

$$D(\theta) \equiv \frac{|p'(\theta)|}{|p'(\theta_o)|} = \frac{p(\theta)}{p(\theta_o)} , \tag{4.66}$$

where the p's in the second form represent rms pressures. In the case of two equal monopoles, the directivity function is the cosine expression of Eqs. 4.62 and 4.65. Usually the directivity function is expressed in decibels by taking 20 times the logarithm of the pressure ratio of Eq. 4.66.

Electrical Steering

Phase differences between radiators are often introduced electricially by means of time delay. The phase angle at any frequency is related to the *time delay*, τ, by

$$\psi = \omega\tau , \tag{4.67}$$

from which it follows that the angle of the principal maximum,

$$\theta_o = -\sin^{-1}\frac{\omega\tau}{kd} = -\sin^{-1}\frac{c_o\tau}{d} , \tag{4.68}$$

is independent of frequency. Thus θ_o is the angle whose sine is the ratio of the time delay, τ, to the time for an acoustic wave to travel between the two sources. This frequency independence of the peak angle is the reason that electrical steering is so popular.

Two Equal In-Phase Sources

If two sources are in phase, then $\psi = 0$ and Eqs. 4.62 and 4.65 reduce to

$$\underline{p}' = 2\underline{p}'_o \cos\left(\frac{kd}{2}\sin\theta\right), \tag{4.69}$$

which has a maximum for $\theta = 0$ equal to the in-phase sum of the two pressures, and a directivity function given by

$$D(\theta) = \left|\cos\left(\frac{kd}{2}\sin\theta\right)\right| . \tag{4.70}$$

This function is plotted in Fig. 4.11 for three values of the parameter kd. Secondary maxima occur when kd is greater than 2π. For values of kd less than unity, the radiation pattern is practically nondirectional.

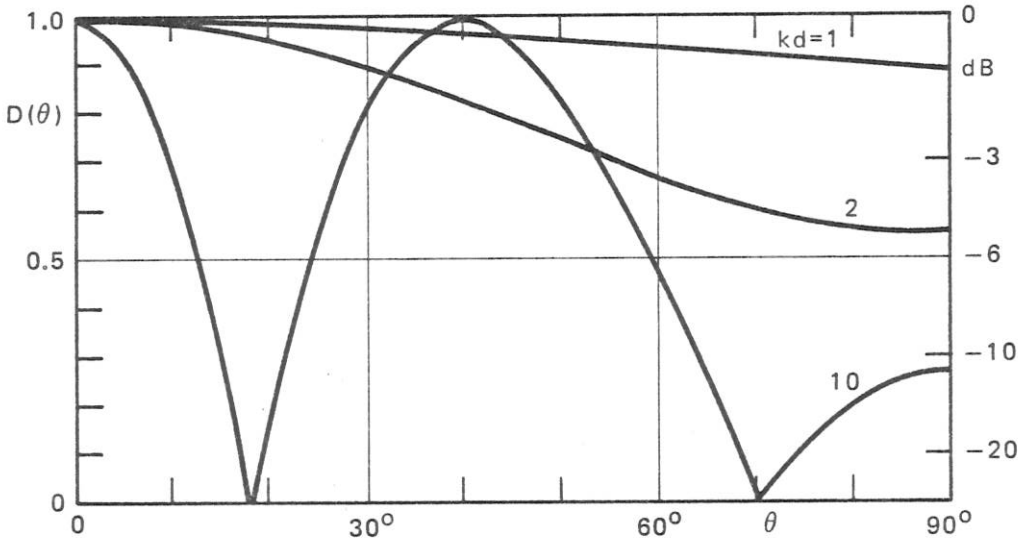

Fig. 4.11. Radiation Pattern for Two Equal In-Phase Monopole Sources

Out-of-Phase Sources

An important special case of two equal sources is that for which the two sources are exactly out of phase with each other. Setting $\psi = \pi$ in Eq. 4.60 leads to

$$\underline{p}' = i\underline{p}'_o\left[\frac{e^{i\beta k\bar{r}}}{1-\beta} - \frac{e^{-i\beta k\bar{r}}}{1+\beta}\right] , \tag{4.71}$$

where the reference pressure, $\underline{p}'_o$, is now

$$\underline{p}'_o = \frac{\omega Q_o}{4\pi\bar{r}} e^{i(\omega t - k\bar{r})} . \tag{4.72}$$

By algebraic manipulation and the use of Eq. 1.59 relating the exponentials to a trigonometric function, Eq. 4.71 can be written in the form

$$\underline{p}' \doteq - \frac{\omega Q_o}{2\pi\bar{r}} e^{i(\omega t - k\bar{r})} \left[\sin(\beta k\bar{r}) - i\beta \cos(\beta k\bar{r}) \right] , \tag{4.73}$$

provided that $\beta < 0.2$.

The approximate expression for the instantaneous pressure for two equal out-of-phase sources given by Eq. 4.73 retains phase information. Of more general interest is the magnitude, P, of the pressure and its relation to that of a single monopole. From Eqs. 4.53 and 4.73,

$$P = \frac{\omega Q_o}{4\pi r} \frac{2}{\sqrt{1 + \left(\frac{d}{2r}\right)^2}} \sqrt{\sin^2(\beta k\bar{r}) + \beta^2 \cos^2(\beta k\bar{r})} , \tag{4.74}$$

where the first term is the magnitude of the pressure from a monopole at the origin. The cosine term is negligible except when the sine term is near zero. The pressure is seen to go through alternate maxima and minima. In the far field, maxima equal to twice the pressure from a single monopole occur whenever $\beta k\bar{r}$ is an odd multiple of $\pi/2$. Minima equal to 2β times the monopole value occur when $\beta k\bar{r}$ is a multiple of π.

Dipoles

A *dipole* consists of two equal out-of-phase radiators whose separation is very small compared to both wavelength and distance to the field point. With this condition both β and βkr are very small compared to unity and Eq. 4.73 becomes

$$\underline{p}' \doteq - \frac{\omega Q_o}{4\pi r} e^{i(\omega t - kr)} \left[kd \left(1 - \frac{i}{kr} \right) \sin\theta \right] . \tag{4.75}$$

In the far field, $kr >> 1$. Dropping the out-of-phase component, Eq. 4.75 then reduces to

$$\underline{p}' = - \frac{\omega^2 Q_o d \sin\theta}{4\pi r c_o} e^{i(\omega t - kr)} . \tag{4.76}$$

The product of the separation, d, and the source flux magnitude, Q_o, is the *dipole strength*, D_o.

The most characteristic aspect of dipole radiation, making it readily recognizable, is the dependence of pressure magnitude on $\sin\theta$. Thus, the directivity function of a dipole is

$$D(\theta) = \sin\theta = \cos\left(\frac{\pi}{2} - \theta \right) . \tag{4.77}$$

The intensity at an angle θ is

$$I(\theta) = \frac{\overline{p'^2}}{\rho_o c_o} = \frac{\omega^4 D_o^2}{32\pi^2 r^2 \rho_o c_o^3} \sin^2\theta , \tag{4.78}$$

and the total power radiated is

$$W_{ac} = 2\pi r^2 \int_0^{\pi} I(\theta) \cos\theta \, d\theta = \frac{\omega^4 D_o^2}{24\pi\rho_o c_o^3} \quad . \tag{4.79}$$

Dipole radiation is of fundamental importance and will be discussed further in Section 9.1.

4.6 Near-Surface Sources

The surface of the ocean is a nearly perfect reflector of sound. As discussed in Section 2.5, radiation from a source near a surface can be analyzed in terms of direct radiation from the source itself and from a negative image source located above the surface, as shown in Fig. 2.3. The strength of the image source is proportional to the specular reflection coefficient, α_r, of the surface and so is a function of its roughness (see Eq. 2.119). The complete radiation pattern is that of two equal out-of-phase monopoles each having a source strength given by that of the image source, plus the field of a monopole of strength equal to their difference.

Surface Image

Figure 4.12 shows the geometrical situation for a source located at a depth h_S below the ocean surface, with a receiver at depth h_R at a horizontal distance r_H from the source. The distances and angles used in the analysis in Section 4.5 are also shown. The rms distance, $\bar{r}$, is given by

$$\bar{r} = \sqrt{r^2 + \left(\frac{d}{2}\right)^2} = \sqrt{r_H^2 + h_S^2 + h_R^2} \quad . \tag{4.80}$$

and the parameter β, which is given by

$$\beta = \frac{rd}{2\bar{r}^2} \sin\theta = \frac{h_S h_R}{\bar{r}^2} \quad , \tag{4.81}$$

is seen to be symmetric with respect to source and receiver depths. The direct distance, r_1, between source and receiver is given by

$$r_1 = \sqrt{r_H^2 + (h_R - h_S)^2} = \bar{r}\sqrt{1 - 2\beta} \quad . \tag{4.82}$$

When the horizontal range is at least twice the source or receiver depth, then β will be less than 0.2 and Eqs. 4.73 and 4.74 can be used to calculate the image contribution. Assuming that the surface is a perfect reflector, the pressure amplitude at the receiver can be approximated by

$$P \doteq \frac{\omega Q_o}{4\pi r_1} 2\sqrt{1 - 2\beta}\sqrt{\sin^2(\beta k\bar{r}) + \beta^2} \quad , \tag{4.83}$$

where the first term is the pressure that would be measured at the receiver if source and receiver were both far from a reflecting surface relative to the distance between them. The remaining terms represent the effect of surface reflection on the received signal.

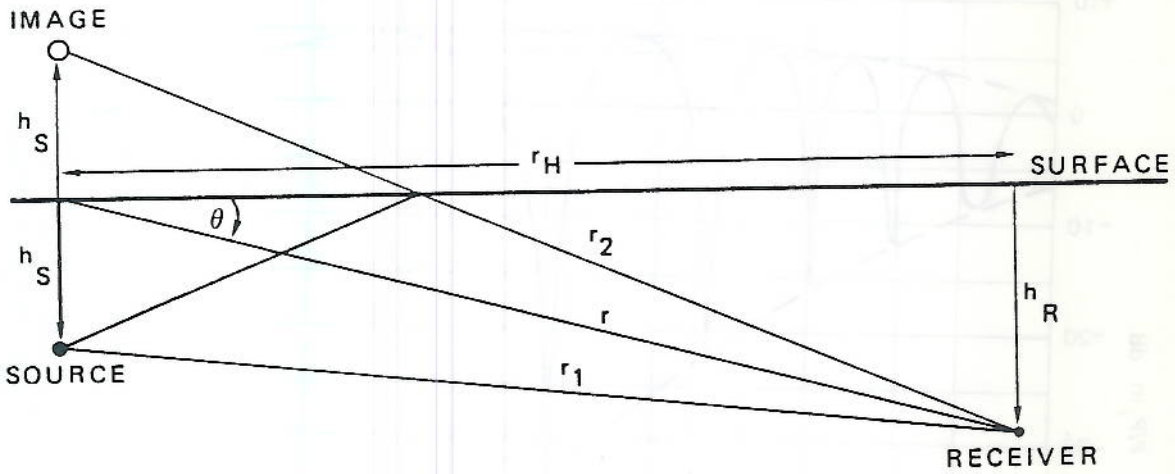

Fig. 4.12. Source and Receiver Near Sea Surface

The effect of a free surface on the received pressure is seen to depend on the values of β and $\beta k\bar{r}$ and therefore on three dimensionless parameters, h_S/h_R, h_R/r_H and kh_S, of which two are defined by the geometry and the third is dependent on frequency.

Interference Patterns

If the source depth is large compared to a wavelength, then βkr may exceed π at close-in distances. In this *near field*, the pressure oscillates rather wildly, between a maximum of almost two times that in an ideal medium and a minimum given by the second term of Eq. 4.83, i.e.,

$$2\beta\sqrt{1 - 2\beta} < \frac{P}{P_i} < 2\sqrt{1 - 2\beta} \quad . \tag{4.84}$$

An example of the resultant interference pattern is shown in Fig. 4.13 as range is increased for fixed source and receiver depths. Similar patterns are obtained by fixing the horizontal distance and changing either source or receiver depths. Varying the frequency changes the number of maxima and minima and also the distances at which they occur.

The region of oscillation is bounded by $\beta k\bar{r}$ equal to $\pi/2$. This occurs where the geometry is such that

$$\frac{h_R}{r_H} \doteq \sin\theta = \frac{\lambda}{4h_S} \quad . \tag{4.85}$$

For angles less than this, i.e., for shallower receiver depths or greater horizontal ranges, the relative level decreases continuously. In the example given in Fig. 4.13 this occurs at a relative range of 20. Beyond a relative range of 60, the level received in the presence of a surface is everywhere less than the free-field value, the discrepancy increasing at a rate of 6 dB per double distance. Thus, when

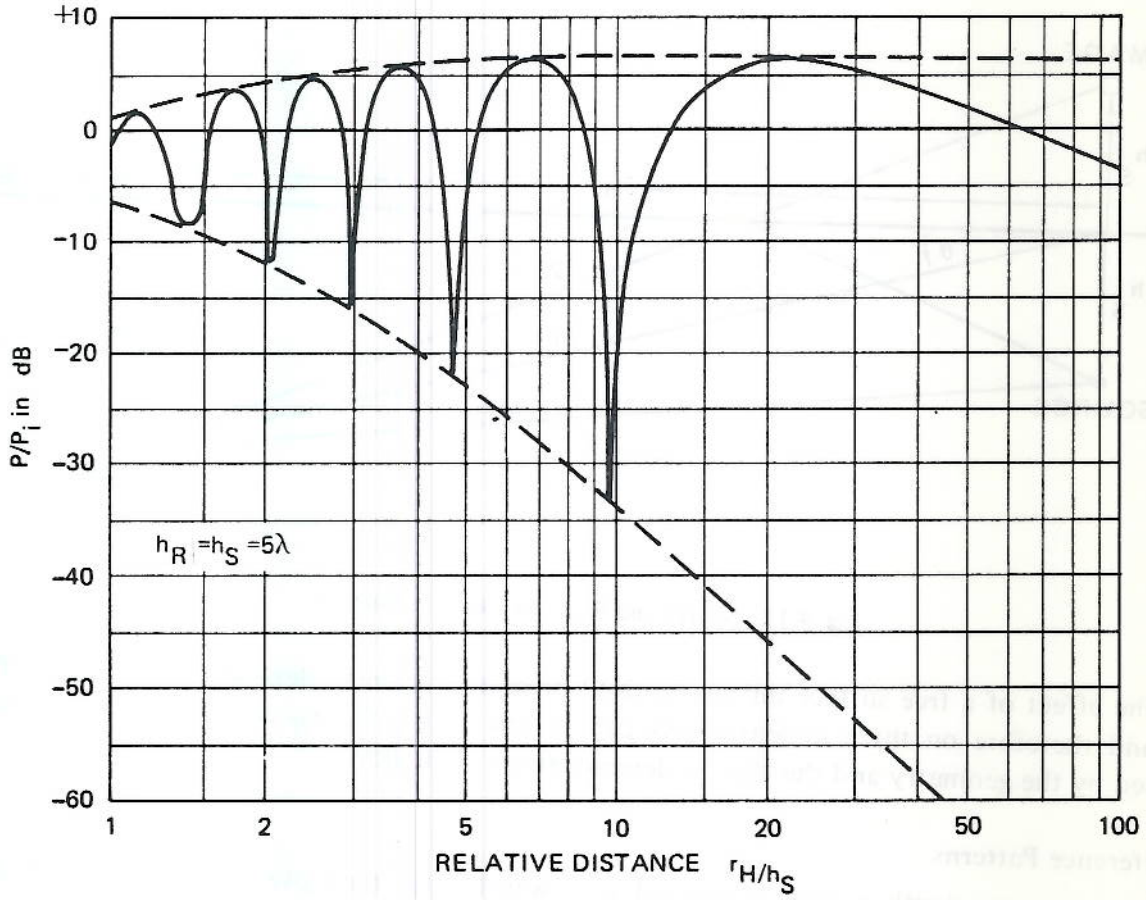

Fig. 4.13. Example of Image Interference

source and receiver are close to the surface, the far-field pressure decreases at a rate of 12 dB per double distance, twice that normally attributable to spherical spreading in an unbounded medium.

The effect at long ranges is appreciably reduced if the surface is rough and only part of the signal is specularly reflected. It can be shown that, when the surface is not perfectly reflecting, the inequality of Eq. 4.84 should be supplemented by another,

$$1 - \left|\alpha_r\right| < \frac{P}{P_i} < 1 + \left|\alpha_r\right| \quad , \tag{4.86}$$

where α_r is the pressure reflection coefficient defined in Section 2.5. Thus, if the reflection coefficient were only 0.9, the anomaly would be limited to 20 dB, and several of the minima in Fig. 4.13 would not be so severe.

Underwater sound pressure fields are affected by surface image interference in many practical situations. Thus, it is not unusual to find interference minima and maxima out to distances of 3 to 5 km from a source. The effects are strongest in the middle frequencies of 300 to 3000 Hz. Above these frequencies, roughness of the surface often tends to wipe out the coherence between source

and image, and the received intensity is nearly twice that for the direct path alone. At lower frequencies, bottom reflections can act to fill in the interference minima.

Effects on Noise Measurements

Measurements of free-field underwater source strengths are often contaminated by free-surface image interference effects. In theory, image interference can be calculated and measured pressures corrected to free-field values. However, as illustrated by Fig. 4.13, the effect is very sensitive to exact values of the parameters. One seldom knows depths or distances with the precision required. One way of avoiding this problem is to average over several cycles of the interference pattern, either by varying the horizontal range during the measurement or by averaging readings of several receivers at a number of depths. When the decibel average of a number of measurements randomly scattered over several interference cycles is taken, the result is generally within ± 0.5 dB of the free-field value. When it is not possible to cover several interference cycles, another approach is to find a maximum of the interference pattern and to estimate the free-field value by subtracting 5 dB from the measured pressure.

Free-field source strengths cannot readily be measured when sources are within a quarter wavelength of the surface. In such cases the surface acts to modify the radiation pattern to that of a dipole, the strength of which is proportional to the product of the monopole strength and distance below the surface of the source. When making low-frequency measurements of such near-surface sources, it is not necessary to know the source depth if what is desired is the dipole source strength. One need merely compute $\sin\theta$ from

$$\sin\theta = \frac{h_R}{\sqrt{r_H^2 + h_R^2}} , \tag{4.87}$$

and correct the measured pressures by this amount. However, if the monopole source strength is to be calculated, then the effective source depth must also be ascertained. This is feasible for relatively small sources but quite difficult for large, distributed sources such as surface ships. If a source depth is assumed, then the complete measurement should specify this depth as well as the monopole source level, since any user of the data will need to know the effective source depth in order to calculate the sound field at a distance.

4.7 Linear Arrays

As an introduction to consideration of distributed sound sources such as pistons it is instructive to develop expressions for the pressure fields of linear arrays of monopoles.

Arrays of Equally-Spaced Monopoles

The expressions derived in Section 4.5 for the pressure field of two equal monopoles can be generalized to any number of equally-spaced sources in a line either by summing the individual contributions from all N elements of an array or by a process of extrapolation from results for a small number of elements. The second method will be developed here.

From Eqs. 4.62, 4.63 and 4.65, the far-field pressure for a two-element array (*two-pole*) can be written

$$\underline{p}'(2) = 2\underline{p}'_o \cos\phi = 2\underline{p}'_o \frac{\sin 2\phi}{2\sin\phi} , \tag{4.88}$$

where

$$\phi \equiv \frac{1}{2}(kd\sin\theta + \psi) = \frac{kd}{2}(\sin\theta - \sin\theta_o) . \tag{4.89}$$

The pressure field for a two-pole is therefore that of a source having peak strength equal to their sum and a directional pattern calculable from

$$D_2(\theta) = \frac{\sin 2\phi}{2\sin\phi} . \tag{4.90}$$

As illustrated by Fig. 4.14, arrays of three, four and five elements can be treated as the sums of monopoles and two-poles all of which have the same origin. Thus, the pressure field of the three-element array of Fig. 4.14b can be expressed as the sum of a monopole and a two-pole, the latter having separation $2d$, as

$$\underline{p}'(3) = \underline{p}'_o(1 + 2\cos 2\phi) = \underline{p}'_o(3 - 4\sin^2\phi) = 3\underline{p}'_o \frac{\sin 3\phi}{3\sin\phi} . \tag{4.91}$$

A four-element array can be treated as the sum of two two-poles, one with separation d and the other with separation $3d$. The resultant pressure is

$$\underline{p}'(4) = \underline{p}'_o(2\cos\phi + 2\cos 3\phi) + \underline{p}'_o(8\cos^3\phi - 4\cos\phi) = 4\underline{p}'_o \frac{\sin 4\phi}{4\sin\phi} . \tag{4.92}$$

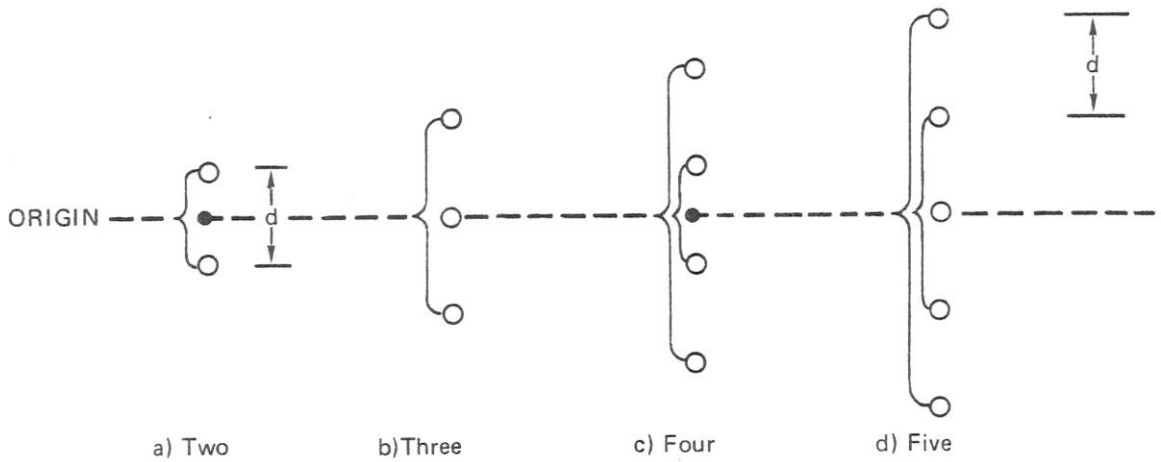

Fig. 4.14. Linear Arrays of up to Five Elements

A similar expression can be derived for a five-element array by summing the fields of a three-element array and a two-pole having a separation between elements of $4d$, as illustrated in Fig. 4.14d. The resultant pressure field is identical to the final form of Eq. 4.92 except that the three 4's are replaced by 5's. Since all of these results are of the same form, it is reasonable to generalize Eq. 4.92 to an N-element array, obtaining

$$\underline{p}'(N) = N\underline{p}'_o \frac{\sin N\phi}{N \sin \phi} , \tag{4.93}$$

which in terms of separation, wave number and steering angle is

$$\underline{p}'(N) = N\underline{p}'_o \frac{\sin\left[\frac{Nkd}{2}(\sin\theta - \sin\theta_o)\right]}{N \sin\left[\frac{kd}{2}(\sin\theta - \sin\theta_o)\right]} . \tag{4.94}$$

The quantity Nd is the effective length, L', of the array, given by the actual length, L, plus one separation, d. If we think of each monopole source as the kernel of a line element of length d centered on the source, then L' is the total length of all of these line elements. The product $N\underline{p}'_o$ is the pressure field that would result if all N of the monopoles were concentrated at the origin. The expression for the rms pressure field of an N-element array is thus

$$p(N) = Np_o D(\theta) , \tag{4.95}$$

where

$$D(\theta) = \left| \frac{\sin\left[\frac{kL'}{2}(\sin\theta - \sin\theta_o)\right]}{N \sin\left[\frac{kd}{2}(\sin\theta - \sin\theta_o)\right]} \right| . \tag{4.96}$$

We will return to this expression after first considering the special case of radiation from a continuous line.

Continuous Line Radiators

While few actual line radiators are continuous, many arrays approximate this condition and it is therefore useful to compute the directivity function for a continuous line. Consider the continuous line radiator sketched in Fig. 4.15. The field point P is considered to be in the far field, i.e., $r >> L$. The pressure at P due to the element dy located y distance from the center of the line, taken to be the origin, can be expressed

$$d\underline{p}' = d\underline{p}'_o e^{ik(r - r')} \doteq \frac{\underline{p}'_o}{L} e^{iky \sin\theta} dy . \tag{4.97}$$

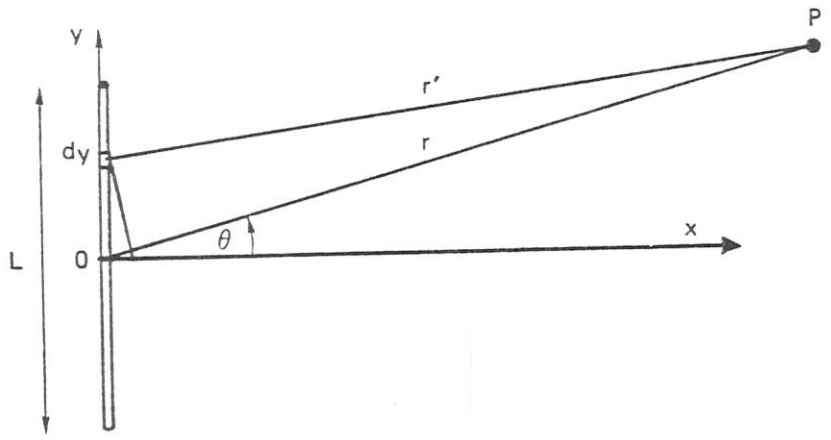

Fig. 4.15. A Continuous Line Radiator

The total pressure at P is the integral of this expression over the length, as given by

$$\underline{p}' = \underline{p}'_o \frac{1}{L} \int_{-L/2}^{L/2} e^{iky \sin\theta}\, dy$$

$$= \frac{\underline{p}'_o}{ik\frac{L}{2}\sin\theta}\left[e^{ik(L/2)\sin\theta} - e^{-ik(L/2)\sin\theta}\right] = \underline{p}'_o \frac{\sin\left(\frac{kL}{2}\sin\theta\right)}{\frac{kL}{2}\sin\theta} . \qquad (4.98)$$

The directivity function for a continuous line array is therefore

$$D(\theta) = \left| \frac{\sin\left(\frac{kL}{2}\sin\theta\right)}{\frac{kL}{2}\sin\theta} \right| = \left| \frac{\sin\overline{a}}{\overline{a}} \right| , \qquad (4.99)$$

where $\overline{a}$ represents the denominator. This same expression can be derived by treating a continuous line radiator as an N-element array in the limit as N becomes very large and d becomes very small. In this limit, $L' \to L$, $\sin\phi \to \phi$ and $N\phi \to \overline{a}$. Equation 4.96 then reduces to Eq. 4.99, provided θ_o is taken to be zero.

The directivity function for a continuous line radiator is plotted in Fig. 4.16, for values of $\overline{a}$ up to 6π. The minor peaks are called *side lobes*. The first side lobe, at $\overline{a} = 3\pi/2$, is down 13.5 dB from the main lobe. The second one, at $\overline{a} = 5\pi/2$, is down 19 dB, and all the others are more than 20 dB below the peak of the pattern. The total width of the main beam is twice that of the side lobes.

Returning to an array of N equally-spaced monopoles, Eq. 4.96 for the directivity function can be written in the form

$$D(\theta) = \left| \frac{\sin \bar{a}}{N \sin \phi} \right| = \left| \frac{\sin \bar{a}}{N\phi} \cdot \frac{\phi}{\sin \phi} \right| = \left| \frac{\sin \bar{a}}{\bar{a}} \right| \div \left| \frac{\sin \phi}{\phi} \right| = \frac{D(L', \theta)}{D(d, \theta)} , \quad (4.100)$$

since $\bar{a} = N\phi$. Thus, the directivity function of an N-element array can be calculated by dividing the directivity function for a continuous line of length $L' = L + d$ by that for a line of length d. As long as ϕ is small, the pattern of the finite-element array is very similar to that for the continuous array. However, when ϕ exceeds about $\pi/4$, side-lobe response of the N-element array becomes larger, and, when $\phi = \pm \pi$ or any multiple thereof, the response equals that of the main lobe. The lowest frequency for which this can happen is that for which

$$\phi = \frac{\pi d}{\lambda} (\sin \theta - \sin \theta_o) = \pi . \quad (4.101)$$

For an array steered broadside, this occurs when the separation between the elements equals a wavelength. If the array is steered to end fire, the second major lobe will first appear for an element spacing of only half a wavelength.

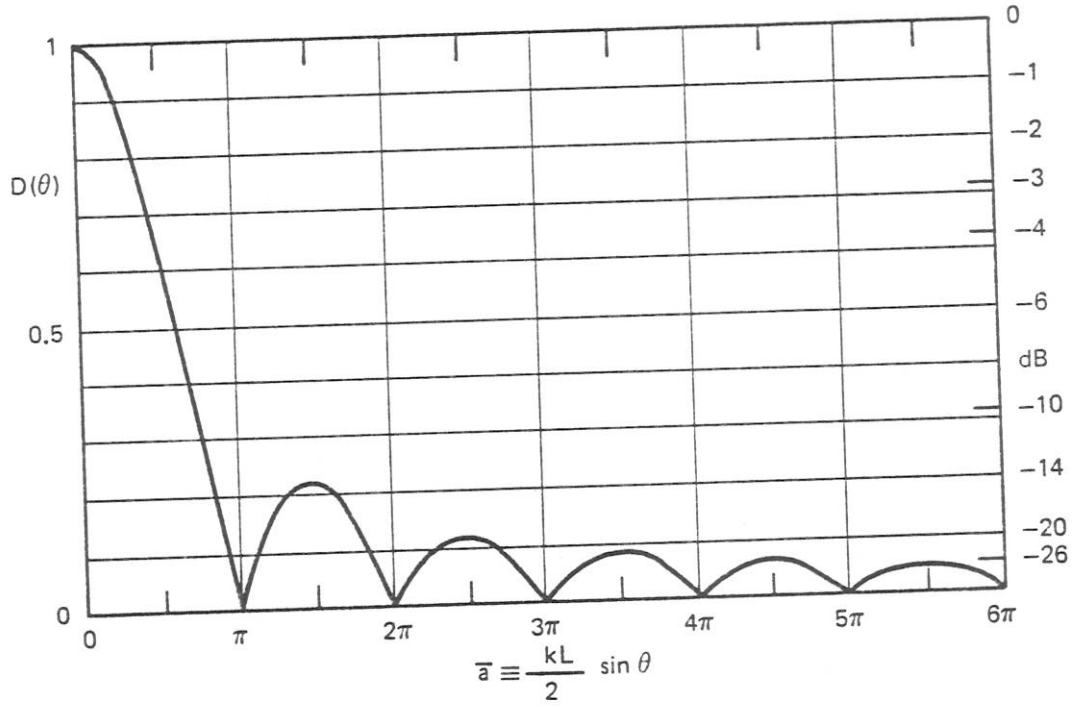

Fig. 4.16. Radiation Pattern of a Continuous Line Array

Directivity Factor

An important measure of the directional characteristics of any radiator is the ratio of the total power radiated to that which would have been radiated if all its strength were concentrated at the origin. This ratio of the average intensity to the intensity at the peak of the main lobe is always less than unity. Its reciprocal is the *directivity factor*, DF, defined by

$$DF \equiv \frac{I(\theta_o)}{\overline{I}} = \frac{4\pi r^2}{\iint_S D^2(\theta)\, dS} \quad . \tag{4.102}$$

A surface element, dS, on a sphere can be expressed by

$$dS = 2\pi r \cos\theta \; r\, d\theta = 2\pi r^2\, d(\sin\theta) \quad , \tag{4.103}$$

whence Eq. 4.102 for the directivity factor can be written

$$DF = \frac{2}{\int_{-1}^{1} D^2(\theta)\, d(\sin\theta)} \quad . \tag{4.104}$$

The directivity factor of a continuous line array steered broadside is

$$DF = \left(\frac{2}{kL} \int_0^{\frac{kL}{2}} \left(\frac{\sin\bar{a}}{\bar{a}} \right)^2 d\bar{a} \right)^{-1} \quad , \tag{4.105}$$

where $\bar{a}$ is used as a dummy variable to represent $kL/2 \sin\theta$, as in Eq. 4.99. For values of $kL < 2$, the radiation is almost omnidirectional and the directivity factor is close to unity. Directionality only becomes dominant for $kL > 4$. For large kL, the integral in Eq. 4.105 equals $\pi/2$ and the directivity factor is given by

$$DF \doteq \frac{kL}{\pi} \qquad (kL > 4) \quad . \tag{4.106}$$

Directivity Index

The logarithmic form of the directivity factor is called the *directivity index*, DI, as defined by

$$DI \equiv 10 \log DF \quad . \tag{4.107}$$

To a close approximation, the DI of a continuous line array, plotted in Fig. 4.17, can be estimated from

$$DI \doteq 10 \log \frac{kL}{\pi} = 10 \log \frac{2L}{\lambda} \quad . \tag{4.108}$$

The directional pattern of an N-element array is essentially the same as that for a continuous line for frequencies such that the element spacing is less than a half wavelength. For these frequencies, the DF and DI are given by Eqs. 4.106 and 4.108 with L' replacing L. For much higher frequencies for which the separation is large compared to a wavelength, the directivity

function is given by that for a continuous line of length L' divided by that for a line of length d, and

$$DF \doteq \frac{DF(L')}{DF(d)} = \frac{\dfrac{kL'}{\pi}}{\dfrac{kd}{\pi}} = \frac{Nd}{d} = N \qquad (d > \lambda) \ . \tag{4.109}$$

The directivity index is then

$$DI \doteq 10 \log N \ . \tag{4.110}$$

Thus, the directivity index of an N-element array is similar to that for a continuous line up to the frequency at which this equals 10 log N. For somewhat higher frequencies, the value stabilizes at 10 log N. This behavior is illustrated in Fig. 4.17 for a 20-element array.

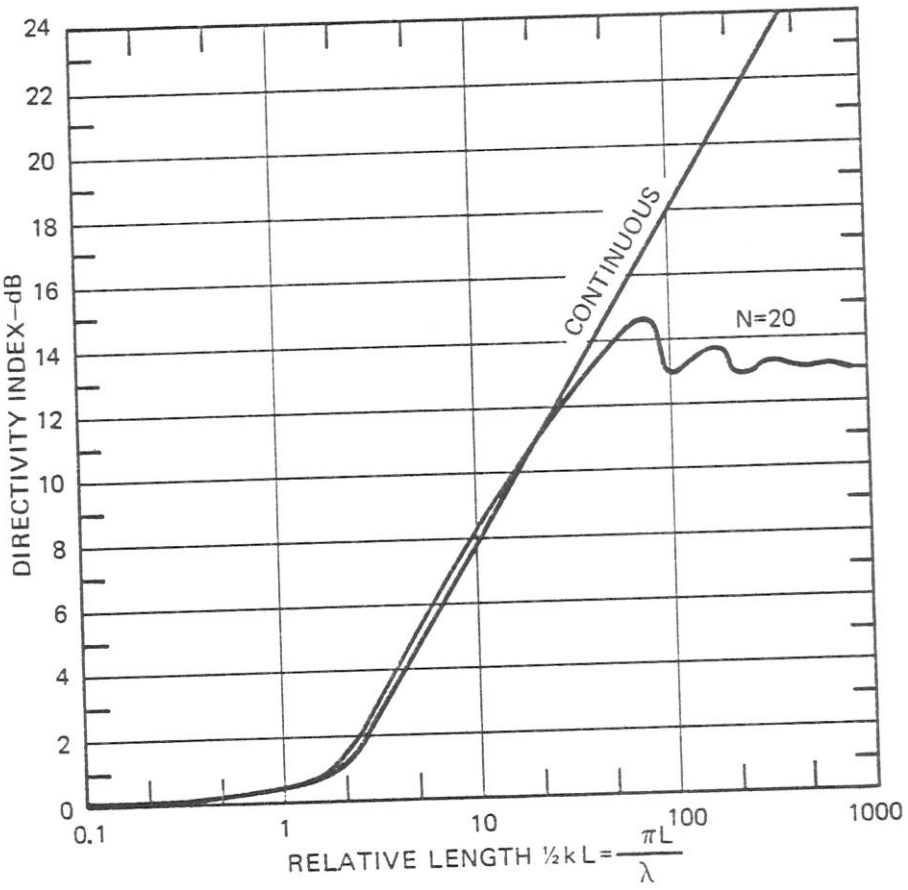

Fig. 4.17. Directivity Index of Line Arrays

Arrays of Directional Sources

The expressions derived thus far apply to arrays of omnidirectional sources. In later chapters we will deal with directive sources, which in some instances may be arranged in an array. If all of the elements of an array of directive sources have the same directivity pattern, then the directivity function of the array is simply the product of the directivity functions of the individual elements and that of an array of omnidirectional sources. Thus, the pattern for an array having an even number of elements, N, can be calculated as a two-pole consisting of directional elements each being formed by a sub-array of $N/2$ elements. Multiplying Eq. 4.88, for a two-element array in which $(N/2)d$ replaces d, by Eq. 4.94, for the directivity of a sub-array of $N/2$ elements, one obtains

$$D_2\left(\frac{N}{2}\right) = \frac{\sin N\phi}{2\sin\dfrac{N}{2}\phi} \cdot \frac{\sin\dfrac{N}{2}\phi}{\dfrac{N}{2}\sin\phi} = \frac{\sin N\phi}{N\sin\phi}, \qquad (4.111)$$

which is the same as the directivity function for an array of N omnidirectional monopoles. Many practical applications follow from the fact that array calculations for omnidirectional sources can be readily extended to arrays of directional sources.

Arrays as Spatial Filters

The principle of reciprocity applies to all linear systems for which the differential equations are symmetric in the spatial variables. As a consequence of this principle, the directional response pattern of a configuration of receivers to incoming plane waves is identical to the radiation pattern of the same configuration of sources. All of the directional patterns derived thus far for radiating monopoles, two-poles and arrays are equally applicable to receiving systems having the same geometry, provided only that the systems are linear.

Passive arrays are used as spatial filters to discriminate against background noise coming from many directions. When sound from a target comes in at the angle of peak response of the main beam, the output of the receiving array will have a higher signal-to-noise ratio than that of a single, omnidirectional receiver by an amount that is the array signal-to-noise gain, usually called the *array gain*. It has been common practice to assume that the dB array gain of an array as a receiver equals its directivity index as a radiator. However, this is not usually true. It would be the case if the background noise were isotropic, i.e., arriving with equal intensity from all directions, but this does not generally occur. The assumption that the passive array gain equals the active directivity index is only valid to the extent that background noise is isotropic.

A number of writers have noted that the mathematical development of array directivity patterns is virtually identical to that for linear filters in spectral analysis. The angular frequency, ω, of spectral theory corresponds to the component of the wave number along the array, i.e., to $k \sin\theta$. Time is analogous to position along the array, and spectral density is analogous to the radiation function. A continuous line array of length L is a spatial analog of a square pulse. Discrete elements correspond to sampling. If the sampling is frequent enough, i.e., if elements are closer than a half wavelength, then the result is virtually unchanged from continuous coverage. If the sampling rate is not sufficient, i.e., if the elements are far apart relative to λ, then extraneous peaks occur.

Just as sampling functions for spectral filters can be designed to achieve specific spectral density functions, so also can linear arrays be designed to achieve desired main-lobe shaping and/or side-lobe reduction. The amplitudes and phases of the individual elements must be controlled in accordance with weighting functions, which functions may be derived from radiation theory or may be taken directly from the signal processing literature. This analogy between signal processing and array spatial filtering is developed more completely in several of the references listed at the end of this chapter.

4.8 Radiation from Rigid Pistons

In the preceding section we dealt with linear arrays of monopoles. However, most radiators of underwater sound occur as surfaces rather than lines. The treatment of surface radiators is essentially the same as that for lines, except that the resultant mathematical functions are usually more complex. In dealing with planar surfaces it is useful to replace the omnidirectional monopole used in array calculations with an elementary piston radiator that radiates sound in only one direction. The radiation pattern of an extended surface is then calculated by integration of the fields of these elementary pistons.

Elementary Piston Radiator

The elementary piston radiator is closely related to the simple pulsating sphere, as can be seen from Fig. 4.18. Since a pulsating sphere radiates sound uniformly in all directions, the placement of a mathematical plane dividing it into two hemispheres has no effect on its field. We may then drop one side, without altering the sound field on the other side, provided we retain the same surface velocity. (Keeping the same flux would involve double the velocity and would produce

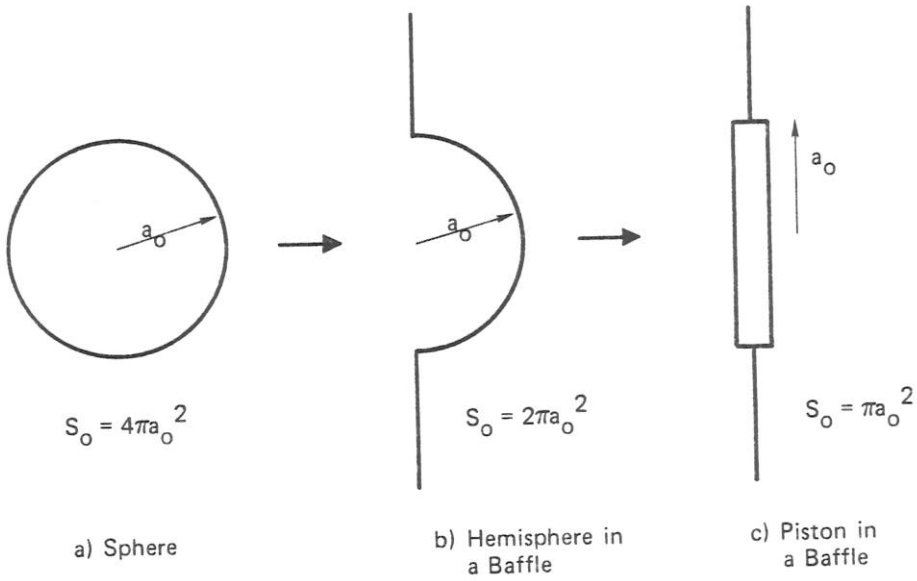

Fig. 4.18. Transformation from Pulsating Sphere to Piston in a Baffle

double the pressure.) It is then a simple step to change from a hemispherical source on a baffle to an equivalent vibrating piston. Since the area is half as great, the same surface velocity produces only half as much oscillating mass flux and half as much sound pressure. It follows that Eq. 4.15 for the pressure field of a monopole can be replaced for an elementary piston by

$$d\underline{p}'(r) = i\frac{\omega\rho_o\underline{u}_o}{2\pi r}e^{i(\omega t - kr)}\,dS \quad . \tag{4.112}$$

In principle, the pressure from any planar source can be calculated by integrating Eq. 4.112 over the surface of the source, taking into account any phase differences between elements.

Circular Piston in a Baffle

The integration of Eq. 4.112 over the area of a uniformly vibrating circular piston is quite similar to the integration carried out in Eq. 4.98 for a continuous line array. Defining $\overline{p}$ as the pressure that would be radiated by a small piston having the same mass flux, the pressure is given by the integral

$$\underline{p}' = \overline{p}\int_S \frac{e^{ik(r - r')}}{r'/r}\,dS \quad , \tag{4.113}$$

where r' is the exact distance from the element to the field point and r is the nominal distance from the center, as depicted in Fig. 4.12 for a line. The integration is carried out in a number of texts, and the far-field result may be written

$$\underline{p}' = \overline{p}\left[\frac{2J_1(ka_o\sin\theta)}{ka_o\sin\theta}\right] \quad . \tag{4.114}$$

The expression in brackets is the pressure pattern of a circular piston in a baffle. It is seen to be similar in form to the $\sin x/x$ function that was found for linear arrays. $J_1(x)$ is the Bessel function of the first order, defined by the series

$$J_1(x) \equiv \frac{1}{2}\left(x - \frac{x^3}{2\cdot 4} + \frac{x^5}{2\cdot 4\cdot 4\cdot 6} - \frac{x^7}{2\cdot 4\cdot 4\cdot 6\cdot 6\cdot 8} + \ldots\right) \quad . \tag{4.115}$$

Setting the denominator of Eq. 4.114 equal to $\overline{a}$, as was done in Eq. 4.99, the directivity function of a circular piston is

$$D(\theta) = \left|\frac{2J_1(ka_o\sin\theta)}{ka_o\sin\theta}\right| = \left|\frac{2J_1(\overline{a})}{\overline{a}}\right| \quad . \tag{4.116}$$

which function approaches unity for small $\overline{a}$, corresponding to omnidirectional radiation in one hemisphere. For large values of $\overline{a}$,

$$D(\theta) \rightarrow \left| 1.6 \frac{\sin(\bar{a} - 0.7)}{\bar{a}^{3/2}} \right| \quad (\bar{a} > 5) \ . \tag{4.117}$$

For medium values, it behaves in a manner similar to that for a line array, as shown in Fig. 4.16, except that the first null occurs at 1.2π, the second at 2.2π, etc.

Many practical sound sources radiate as pistons having values of $ka_o < 2$, for which the directivity function can be expressed as the first three terms of a power series, as

$$D(\theta) = 1 - \frac{(ka_o \sin\theta)^2}{8} + \frac{(ka_o \sin\theta)^4}{192} \qquad (a < 2) \ . \tag{4.118}$$

Half of the total power radiated is contained in a cone defined by $ka_o \sin\theta \doteq 1.6$.

Near Field of a Piston Radiator

The expression in Eq. 4.114 for the radiated pressure of a piston source was derived under the assumption that the difference between r' and r is small compared to either distance. In practice, this expression for pressure agrees well with measurements for distances that satisfy the relationship

$$(kr) > (ka_o)^2 \ . \tag{4.119}$$

which inequality defines the *far field*. The *near field* is quite complicated, often involving interference minima and maxima. However, for pistons having $ka_o < \pi$ there are no interference patterns and the intensity and pressure fields are continuous.

Close to the surface of a piston source, i.e., when $r < a_o$, the pressure on the axis is

$$\underline{p}'(r < a_o) \doteq 2\rho_o c_o u_o \, e^{i\omega t} \sin\left(\frac{ka_o}{2}\right) \ ; \tag{4.120}$$

hence, the on-axis pressure at a large distance r is related to the near-field pressure by

$$\frac{\underline{p}'(r > a_o)}{\underline{p}'(r < a_o)} \doteq i \frac{\left(\frac{ka_o}{2}\right)^2 e^{-ikr}}{(kr)\sin\left(\frac{ka_o}{2}\right)} \ . \tag{4.121}$$

For the small values of ka_o that are often found when dealing with ship radiation, the sine term in Eq. 4.121 can be replaced by its argument, and the rms pressure in the far field is then related to its near-field value by

$$\underline{p}(r > a_o) \doteq \underline{p}(r < a_o) \frac{a_o}{2r} \qquad (ka_o < 1) \ . \tag{4.122}$$

A practical consequence of Eq. 4.122 is that, for values of ka_o typical of many radiations from ship hulls, pressure measurements made close to the hull are representative of far-field values. This

experience is contrary to that of the transducer community, since most transducers are highly directional devices that operate at high values of ka_o for which the near field is very complicated.

Radiation Impedance and Efficiency

Pressure is not constant over the surface of a piston. Values given by Eq. 4.120 apply only near centers of pistons. To find the reaction force experienced by a piston due to its motion, one must find the average pressure over the entire piston surface. The general expression involves two types of Bessel functions. The resultant values for the specific radiation resistance and reactance are plotted in Fig. 4.19. For pistons satisfying the requirement that $ka_o < 1$, the specific radiation resistance is

$$\sigma_r = 1 - \frac{J_1(2ka_o)}{ka_o} \doteq \frac{(ka_o)^2}{2}\left[1 - \frac{(ka_o)^2}{6}\right], \tag{4.123}$$

and the reactance is

$$\sigma_x \doteq \frac{8}{3\pi}(ka_o)\left[1 - \frac{(2ka_o)^2}{15}\right]. \tag{4.124}$$

It follows that for small values of ka_o the radiation efficiency is proportional to the first power of ka_o,

$$\eta_{rad} \doteq \frac{3\pi}{16} ka_o \qquad \left(ka_o < \frac{1}{2}\right), \tag{4.125}$$

as one would expect for a monopole type of radiation.

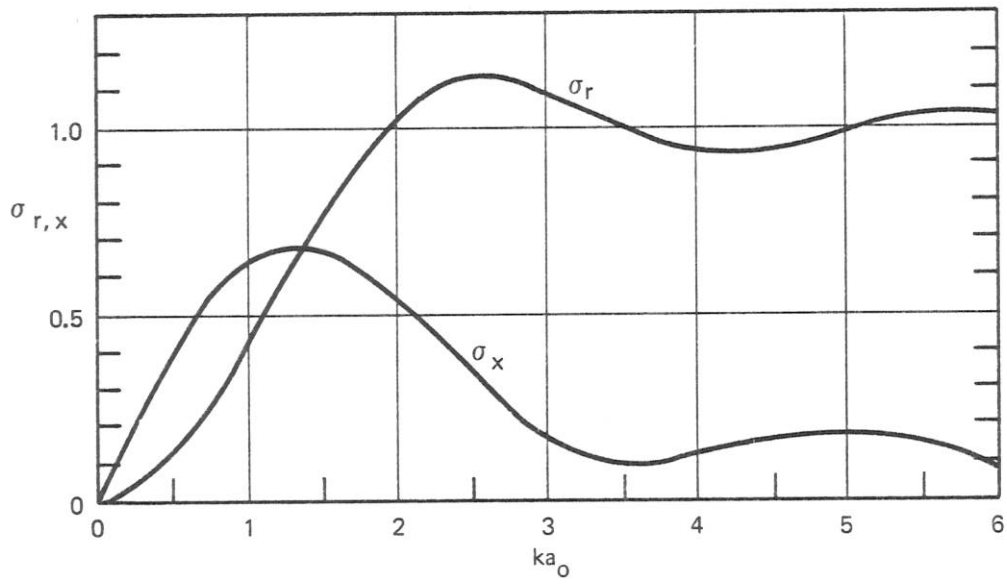

Fig. 4.19. Specific Impedances of Circular Pistons

Directivity Factor and Index

The directivity factor for a piston radiator is calculated by substituting the directivity function, $D(\theta)$, given by Eq. 4.116, into Eq. 4.102 and carrying out the integration. The result is

$$DF \equiv \frac{I(0)}{\overline{I}} = \frac{(ka_o)^2}{1 - \dfrac{J_1(2ka_o)}{2ka_o}} = \frac{(ka_o)^2}{\sigma_r} \quad . \tag{4.126}$$

For values of ka_o up to about 1, $DF \doteq 2$, representing essentially omnidirectional radiation in one hemisphere and zero radiation in the other. For $ka_o \geqslant 2$, σ_r is close to unity, as shown in Fig. 4.19, and

$$DF \doteq (ka_o)^2 \qquad (ka_o \geqslant 2) \quad . \tag{4.127}$$

The directivity index of a piston radiator is therefore 3 dB at low frequencies and is given by

$$DI = 20 \log ka_o = 20 \log \frac{2\pi a_o}{\lambda} \tag{4.128}$$

at high frequencies.

Pistons of Other Shapes

The above development applies only to circular pistons. Many ship radiating surfaces are more nearly rectangular. For rectangular pistons of dimensions $2a \times 2b$ the directivity function is the product of two $\sin \overline{a}/\overline{a}$ functions, one for each dimension. Molloy (1948) calculated the directivity index and found that at high frequencies it can be estimated from

$$DI \doteq 1.2 + 10 \log ka + 10 \log kb \quad . \tag{4.129}$$

Stenzel (1939) has shown that for many different shapes the main beam pattern is represented by

$$D(\theta) \doteq 1 - \frac{1}{2} k^2 L_x \sin^2 \theta \quad , \tag{4.130}$$

where L_x is the area moment of inertia about an axis perpendicular to the direction of the pattern. L_x equals $(a/2)^2$ for a solid circle, $(a^2/2)$ for a ring, and $(a^2/3)$ for a square piston having sides of length $2a$. Since acoustic calculations usually need not be very precise, it follows that equations for circular pistons can be used, provided the aspect ratio of the radiator is close to unity.

Planar Arrays

It has been demonstrated that the directivity patterns of continuous line radiators are similar to those for linear arrays having their elements closer than a half wavelength. In the same way planar arrays of discrete radiators have radiation patterns similar to those of pistons. Directivity

indices of planar arrays of pistons are given by Eq. 4.129 up to a limit 3 dB higher than 10 log N, the limit that applies for unbaffled omnidirectional sources.

Pistons in Non-Rigid Baffles

In the discussion thus far it has been assumed that the baffle is rigid. This is almost always a good approximation in air, but not as true in water. Feit and Duncan (1968) have considered the effect of finite baffle impedance on piston radiation impedance and found that both the resistance and reactance are reduced for $ka_o < 1$. For ka_o up to about one half, they found that Eq. 4.123 can be replaced by

$$\sigma_r = \frac{(ka_o)^2}{2}\left[1 - \frac{\gamma_b}{ka}\tan^{-1}\left(\frac{ka_o}{\gamma_b}\right)\right] , \tag{4.131}$$

where

$$\gamma_b \equiv \frac{\rho_o a_o}{\mu_b'} , \tag{4.132}$$

and μ_b' is the mass area density of the baffle. Taking h to be the baffle thickness,

$$\frac{\gamma_b}{ka_o} = \left(\frac{\rho_o a_o}{\rho_b h}\right)\left(\frac{c_o}{\omega a_o}\right) = \frac{\rho_o c_o}{\omega \rho_b h} , \tag{4.133}$$

where ρ_b is the density of the baffle material and $\omega\rho_b h$ is the baffle mass reactance per unit area. It is apparent that for a given baffle the effect of finite baffle impedance is pronounced at low frequencies, and that at high frequencies the baffle appears to be rigid. It is essentially a question of the relative impedances of the medium and the baffle.

Unbaffled and Partially Baffled Pistons

The importance of the baffle to piston radiation can be appreciated by considering unbaffled and partially baffled pistons. Morse and Ingard (1968) show that the pressure pattern at large distances from a free-floating, vibrating disk is equal to that of a piston in a baffle multiplied by $\cos\theta$. At high frequencies, for which $ka_o >> 1$, the extra $\cos\theta$ has little effect and the pattern ahead of the disk is unchanged. Since radiation occurs behind the disk equal to that in front, though out of phase by 180°, the radiation resistance at high frequencies is double that for a baffled piston.

At low frequencies, for $ka_o < 1$, the $\cos\theta$ term dominates the radiation pattern of the free disk, and it radiates as a dipole. In the limit, for small ka_o, the radiation efficiency is given by

$$\eta_{rad} \doteq \frac{1}{2}(ka_o)^3 , \tag{4.134}$$

and unbaffled disks are seen to be much less efficient as radiators of sound than are pistons in infinite baffles.

The question of baffle size required to achieve much of the effect of an infinite baffle was examined by Crane (1967). He carried out calculations for circular pistons of radius a_o in circular

baffles of radius r_b, and found that the radiation impedance is virtually equal to that for an infinite baffle provided $kr_b > \pi$, i.e., that the baffle diameter is greater than a wavelength.

Pistons on Non-Planar Baffles

In practical marine acoustics, piston-like radiating surfaces occur on finite curved bodies rather than in plane baffles. While the general case has not been treated mathematically, examples of pistons in rigid cylinders and spheres have been treated in the literature. The calculations involve Legendre and Bessel functions of various orders and are quite complex.

Morse (1948) considered a piston of radius $a_o = a \sin \phi_o$ in a sphere of radius a. He found that the equivalent source strength is somewhat greater than that for a piston in a plane baffle, and that for moderate angles, up to 60°,

$$Q_{eq} \doteq \frac{1}{\cos^2 \frac{\phi_o}{2}} Q \quad . \tag{4.135}$$

His calculations also show that a change from plane to spherical baffle makes a large change in the angular distribution of the radiated sound pressure, but has relatively little effect on the average radiation impedance load of the piston.

Laird and Cohen (1952) were the first to solve the problem for pistons on cylinders, but did not report any simple relation to piston radiation in planar baffles. Greenspon and Sherman (1964) found that, for a piston set in a cylinder, the pressure distribution along the generator agrees well with that for a plane, while around the periphery it is in excellent agreement with that for a sphere. In all cases, the pressure distribution depends on both the ka of the piston itself and that of the curved body, while total radiated power and average intensity are much the same as those for a piston in a plane.

Effect of Flow on Piston Radiation

Since ships are usually in motion, it is pertinent to investigate any effects which flow past a piston might have on its radiation. Chetaev (1956) calculated the acoustic impedance of a square piston in an infinite baffle radiating into a moving medium. He found negligible effects on both the resistive and reactive components provided the product of ka_o and the Mach number, M, is small compared to unity. Thus, for speeds found in water, the effect should only be noticeable at very high frequencies.

4.9 Radiation from Hull Openings

Usually when dealing with pistons as sound sources one thinks in terms of oscillating rigid plates. At low frequencies, however, pulsating fluid motions in hole openings also generate sound by the same mechanism. This can be understood by thinking of a rigid piston as a device that causes the fluid in front of it to move back and forth, thereby radiating sound. The same oscillating motion can occur in an opening due to pressure pulsations in a tank or pipe. In ship systems, such pulsations occur in hull openings such as those connected with seawater piping systems and tanks, as well as propulsion system exhausts.

Radiation from Pipe Ends

The inlet and discharge lines of seawater pumps may be treated as open-ended pipes in essentially infinite baffles. Morse (1948) has shown that the radiation from an opening in a wall is the same as that from a massless piston set in the wall and having the same mass flux. The expressions given in the previous section for piston radiation therefore apply unaltered to pipe endings. The problem reduces to finding the mass flux, Q.

In the case of piping systems it is common practice to measure the rms oscillating pressure, $\overline{p}_i$, inside the pipe. If this is measured within an eighth of a wavelength of the opening, then the rms fluctuating fluid velocity, $\overline{u}$, is related to it through the impedance of the opening, as

$$\overline{u} \doteq \frac{\overline{p}_i S}{|Z_r|} = \frac{\overline{p}_i S}{\sqrt{R_r^2 + X_r^2}} = \frac{\overline{p}_i}{\rho_o c_o \sqrt{\sigma_r^2 + \sigma_x^2}} \tag{4.136}$$

The components of the radiation impedance are given in Fig. 4.19 and by Eqs. 4.123 and 4.124.

The assumption of constant velocity, $\overline{u}$, across the mouth of the opening is valid only for low frequencies for which the pipe diameter is small compared to a wavelength. For $ka_o < 1/2$, Eq. 4.136 reduces to

$$\overline{u} \doteq \frac{\overline{p}_i}{\rho_o c_o \sigma_x \sqrt{1 + \left(\frac{\sigma_r}{\sigma_x}\right)^2}} \doteq \frac{3\pi \overline{p}_i}{8\rho_o c_o k a_o} , \tag{4.137}$$

from which the rms radiated sound pressure is

$$p(r) \doteq \frac{3\pi}{16} \frac{a_o}{r} \overline{p}_i D(\theta) . \tag{4.138}$$

The directivity function, $D(\theta)$, is the approximate expression given by Eq. 4.118. At low frequencies the power radiated is

$$W_{ac} = \eta_{ac} \overline{p}_i \overline{u} S_o \doteq \frac{1}{2} \left(\frac{3\pi}{8}\right)^2 \frac{\overline{p}_i^2 S_o}{\rho_o c_o} , \tag{4.139}$$

showing that the power for a given pipe pulsation pressure is proportional to the area of the opening but is independent of ka_o.

Radiation from Tank Resonances

When they occur, flow-excited cavity resonances of ship and submarine tanks produce very strong tonal components. All open-mouth cavities have resonant frequencies. The fluid in the opening moving in and out provides the mass, while compressibility of the cavity volume acts as the spring. In air, i.e., in *Helmholtz resonators*, compressibility is provided by the gas in the resonator. In liquids, which are virtually incompressible, flexibility of the tank walls provides the spring action. Sometimes tanks are only partially filled with liquid, in which case the gas volume is the compressible member.

Cavity resonances can be excited in a number of ways, but by far the most important is flow

excitation. As discussed in Chapter 9, all wake flows are unstable, shedding vortices at frequencies controlled by flow speed and body dimensions. Such vortices occur in cavity openings when fluid flows past the cavity mouth. When the vortex shedding frequency approaches the resonance frequency of the cavity, the cavity begins to pulsate, strengthening the vortices and further increasing the pulsation velocity. The amplitude builds up until it is limited by non-linear effects. Not only does such a flow-excited resonance radiate a very strong tonal component, but also pressures inside the tank may be sufficient to cause fatigue cracking of the tank plates.

When flow-excited tank resonances are found in marine vehicles, they are readily corrected. Redesign of the cavity opening to change the vortex excitation frequency is one cure. Another is addition of reinforcing beams to the tank plates to decrease their flexibility and thereby increase the resonance frequency. Also, flow diverters can be introduced ahead of the tank opening, causing the flow to avoid the opening and thereby reducing both the strengths and frequencies of the vortices.

Radiation from Exhaust Pipes

Pulsating exhaust flows from tail pipes of torpedoes and other underwater exhaust systems also radiate as monopoles. Even though unflanged, such open-ended pipes radiate as though baffled, with the pipe wall providing the baffle. At low frequencies sound is radiated equally in all directions. The radiation reactance is about 30% less, and the pressure about 1.5 dB lower, than that for an opening in a flat surface.

Ffowcs Williams (1969) and Plett and Summerfield (1974) have shown that even for jet engines in air, monopole sources dominate at low Mach numbers. Westervelt and McQuillin (1957) reported that at low frequencies sounds from pulse jets are controlled by volume pulsations. At higher frequencies, dipole and quadrupole radiations are observed. Marine vehicle exhaust systems are similar in many ways to low Mach number pulse jets; monopole radiation can therefore be expected to dominate.

4.10 Radiation from Arbitrary Bodies

While many practical sound sources can be understood in terms of the relatively simple configurations discussed earlier in this chapter, there are other types of radiators which are more complicated. Numerous papers have been published dealing with one or more specific configurations. The present section deals briefly with several methods that are used in calculating the sound fields radiated by arbitrary bodies, and the next section discusses their application to hull radiation problems.

Integral Equation Methods

Solutions of Helmholtz's equation, Eq. 2.61, for acoustic fields radiated by arbitrary bodies can be expressed in terms of integrals over their surfaces. The approach used parallels that originally developed for solving Laplace's equation when presented with a set of arbitrary boundary conditions.* The fact that acoustics formulations deal with retarded time and must retain phase information makes acoustics problems somewhat more difficult than the usual boundary-value problems of potential theory. Were it not for the availability of high-speed computers, this approach would have little appeal.

*See, for example, Kellogg (1953).

Most integral methods start with the *Helmholtz integral equation*, derived by applying Green's theorem to acoustic potentials. In its most common form, the radiated pressure is expressed as a sum of two integrals:

$$\underline{p}'(r) = \int_S \frac{e^{-ikr}}{4\pi r} \left.\frac{\partial p'}{\partial n}\right|_S dS - \int_S p'(S) \frac{\partial}{\partial n}\left(\frac{e^{-ikr}}{4\pi r}\right) dS \quad . \tag{4.140}$$

Solution of this equation requires knowledge of the pressure distribution and of its normal derivative, both evaluated just outside the surface. From Eq. 2.47, the normal pressure gradient at a surface is related to the surface velocity, u, by

$$\left.\frac{\partial p'}{\partial n}\right|_S = \rho_o \frac{\partial u}{\partial t} = i\omega\rho_o u = i\omega_o c_o k u \quad . \tag{4.141}$$

The first integral therefore expresses the monopole field of the surface velocity distribution, while the second can be interpreted as the dipole field of the surface pressures. If both surface velocity and pressure distributions are given, then Eq. 4.140 can be used directly. However, usually only one of these is known and equations must be found to relate the unknown quantity to the known one. In solving these supplementary integral equations, difficulties in the form of indeterminacies occur at certain wave numbers. Chertock (1964, 1970 and 1971) has developed several practical computational procedures for overcoming these problems. Other methods for using integral equations have been published by Copley (1967, 1968) and Schenck (1968).

The most successful applications of integral methods have been in calculating the fields of large complex transducers and of cylindrical shells. Readers interested in further discussion of this subject are referred to the articles and reports listed at the end of this chapter, especially Chertock's (1971) overview.

Spheroidal Wave Functions

Many radiators for which sound fields are desired are cigar-shaped. Rather than carry out the integrals of Eq. 4.140, it is more appropriate to express the sound fields of such bodies in terms of known mathematical functions, of which prolate spheroidal functions are the most useful. In this approach, the geometric outline of the body is fitted as well as possible by a prolate spheroid, and the surface velocity distribution is expressed by a finite series of spheroidal surface functions, as given by Morse and Feshbach (1953). The radiated field is then given by a series of spheroidal wave functions, in much the same manner as in the treatment of a general spherical radiator discussed in Section 3.3. Chertock (1961) developed expressions for the pressure field, radiation impedances and directivity factors for spheroidal modes, and applied these results to consideration of rigid-body and "accordion-like" vibrations of thin prolate spheroids. The usefulness of this approach depends both on the degree of fit of the actual body by a spheroid and the number of terms required to match the surface velocity distribution. It is therefore most useful when treating bodies of revolution at low frequencies.

Slender Body Theory

A weakness of the spheroidal function method is that it assumes bow-stern symmetry. Pond

(1966) overcame this difficulty by representing relatively thin bodies of revolution by distributions of monopoles and dipoles on the body axis. The strengths of the sources are adjusted to produce streamlines that coincide with the hydrodynamic flow over the body. Pond found that bow-stern assymmetries introduce a number of important terms that are not part of a symmetric analysis. Chertock (1964) noted that at low frequencies the far-field radiation pattern is symmetric even though the body itself is not. Thus, the longitudinal *accordion* mode, which radiates strongly along the axis of the body, radiates sound almost equally in the bow and stern directions.

Chertock (1975) has developed a relatively simple method for calculating the radiation fields of slender bodies at very low frequencies. He assumed that the acoustic wavelength is larger than any distance along the body in which the motion changes appreciably. This implies that the fluid can be treated as incompressible when relating the surface velocity and pressure distributions. In fact, the local surface pressure is then simply the fluid density times the local surface acceleration. Chertock has successfully applied this method to the calculation of low-frequency fields of a number of ship-like structures.

Radiation from Cylinders

Slender body methods are most useful at the lowest frequencies. At somewhat higher frequencies, sound radiation from marine vehicles often has characteristics that are similar to those found when treating radiation from cylinders. In this medium frequency range, shell resonances play an important role, and much of the literature relating to cylinders is concerned with these resonances. The subject has offered considerable challenge to theoreticians and most of the papers are highly mathematical. Heckl (1962) summarized the results for finite cylindrical shells in air. He noted that while ring stiffness controls at low frequencies, the results are in good agreement with flat-plate calculations when the circumference of the cylinder exceeds the wavelength of longitudinal waves in the shell.

Junger (1975) pointed out that submergence of a structure in a liquid changes the nature of the problem. In air, the vibration can be calculated as for a vacuum and the radiation then derived from the vibrational pattern by any of a number of acoustic methods. In a liquid, on the other hand, motion of the fluid must be included in dealing with the structure, i.e., one is dealing with a coupled structural-acoustics problem. Junger (1952) has solved the coupled equations for thin, elastic cylindrical shells, finding as much as a 50% change in some resonances. He extended this approach in 1954 to cylinders with reinforcing rings and bulkheads. Different methods of solving the same problems have been developed by Warburton (1961) and by Bleich and Baron (1954, 1965).

It is the author's experience that most of the acoustic characteristics of radiating underwater systems can be understood without resort to detailed analyses of cylindrical structures. Furthermore, the mathematical complexity of these analyses tends to hide some of the basic physics. For these reasons, no details on this subject are given in the present volume. Readers who wish to pursue this subject further may do so by reading some of the articles already mentioned, as well as several others listed at the end of the chapter.

Finite-Element Methods

The finite-element approach to structural-acoustics problems has gained increasing favor as industry has developed larger and faster digital computers. In this approach one divides the structure into a large number of relatively simple sections so chosen that their independent vibrational and radiational characteristics are known. A series of coupled equations is written and

the resultant matrix solved on a high-power computer. The larger the number of equations, the better the results. An application of this method to hull vibrations has been published by Greenspon (1963). MacNeal (1962) has written on the analogy of mechanical and electrical finite elements and the use of electric circuit theory to analyze complex structures. Before the development of high-speed digital computers, vibration problems were often solved by means of finite elements and their electric analogs.

4.11 Radiation from Hulls

The hulls of most marine vehicles are extremely complicated structures that can be excited into vibration, and consequently radiate sound, over a wide range of frequencies. In later chapters we will discuss a number of hydrodynamic and mechanical forces that cover the entire spectrum from as low as 1 Hz to as high as 20 kHz. Calculation of the resultant hull vibration and radiation by any single method seems virtually impossible. Most of the more important characteristics of hull vibrational response and radiation can be understood by dividing the spectrum into a few distinctive frequency regimes, treating each regime by relatively simple physical models.

Definition of Frequency Regimes

Parameters that are most useful in dividing the spectrum into frequency regimes are ratios of the acoustic wavelength to various hull dimensions. Pertinent dimensions are overall length, diameter or width, lengths of compartments, frame spacings and plate thicknesses. The author has found it useful to think in terms of the three basic frequency ranges summarized by Fig. 4.20.

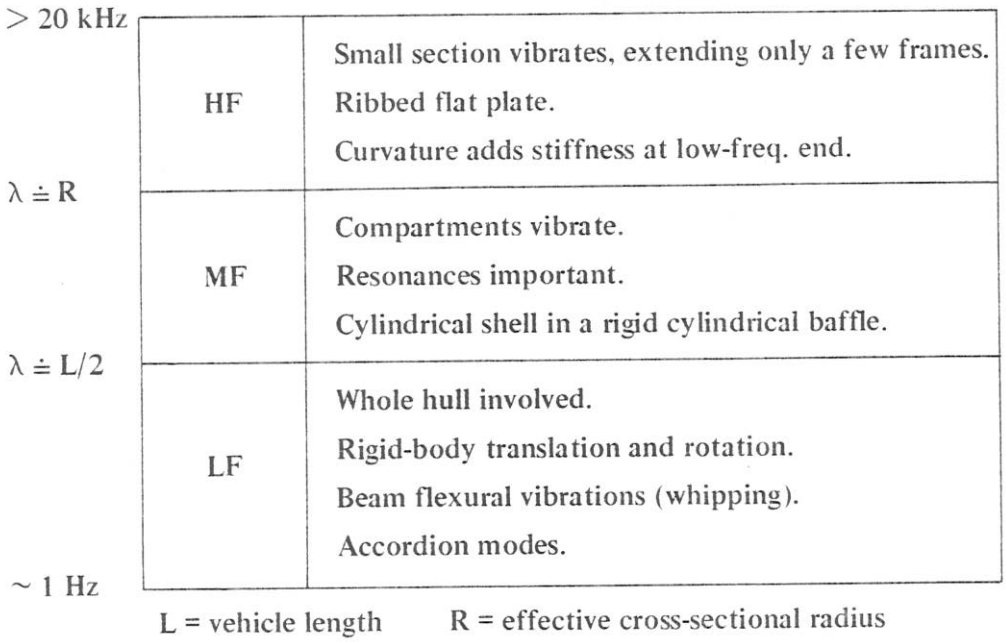

Fig. 4.20. Frequency Regimes for Hull Vibrations and Radiation

Low Frequencies

The *low-frequency* (LF) regime extends from 1 Hz up to the frequency for which the acoustic wavelength equals half the vehicle length. For a vehicle 150 m long, this includes all frequencies up to about 20 Hz. In this regime, the entire hull participates in the motion and applicable models must represent the whole body. Three distinct types of motion may occur at low frequencies, each of which radiates sound with different characteristics. The body may experience rigid-body motion in which it retains its exact shape and either vibrates in position in response to an external alternating force or rotates about an axis. The second type is beam-like flexural bending vibrations, sometimes called *whipping* motions. Finally, there may occur dominantly longitudinal vibrations in which the two ends move out of phase in an accordion-like motion. Expansion and contraction, i.e., breathing, motions of the hull sections are associated with the latter type of vibration.

Low-frequency motions of surface ships are important to naval architects because they are sometimes strong enough to cause damage and because they can be very unpleasant to experience. However, acoustic radiation from these motions is generally negligible. The reason is that the ocean surface acts to reduce the sound by providing negative image sources within a half wavelength of the hull sources, thus partially cancelling them. Thus, any near-surface oscillating-volume source radiates as a dipole, while dipole sources radiate as quadrupoles. Also, as will be discussed in Chapter 8, direct radiation by propeller cavitation generally dominates in this frequency region. Low-frequency radiation is much more important for submerged vehicles, for which image cancellation is much reduced and for which propeller cavitation may be absent.

Methods for calculating low-frequency sounds from submerged bodies were discussed in the previous section. Additional material pertinent to flexural vibrations of hulls and the attendant radiation is presented in the next chapter.

Medium Frequencies

The *medium-frequency* (MF) region of the spectrum applies between the LF region and the frequency for which the acoustic wavelength equals the effective radius of the cross section. Thus, for a circular hull 10 m in diameter, this covers frequencies up to about 300 Hz. In this regime, response to excitation is usually limited to one compartment; the remainder of the hull acts as a baffle.

Individual hull resonances play a major role in the response of the hull to exciting forces and are therefore important in acoustic calculations for the MF range. Resonance frequencies can be estimated from results for cylinders, but are best calculated by finite-element methods. In many ways the decade of frequency covered by this regime is the most difficult part of the spectrum for vibration and acoustics calculations. Slight alterations in the structure that change a resonance frequency by only a few percent result in entirely different responses to specific forcing frequencies. The role of resonances in this frequency regime is clearly indicated in hull structural and acoustic measurements, such as those reported by Donaldson (1968).

High Frequencies

In the *high-frequency* (HF) region, each exciting force causes only a small area to vibrate and the remainder of the hull is effectively an infinite baffle. Radiation in this frequency region can be treated in terms of plate theory. This topic is covered in Chapter 6, where it is shown that ribs play a much more important role than plate curvature. In this frequency regime, the densities of resonances are of greater interest than are their exact frequencies. In fact, sufficient numbers of

resonances occur to enable application of statistical energy methods. In this regime, sound radiation is controlled by plate thicknesses and frame spacings, and the results are only slightly influenced by the overall shape of the hull.

Excitation forces at high frequencies sometimes occur at a single point, such as at a machine foundation. Sometimes they are distributed over wide areas, as in the case of boundary layer turbulence. Both situations are discussed in Chapter 6.

REFERENCES

Sections 4.1 and 4.2

Junger, M.C. and Feit, D., *Sound, Structures and Their Interaction*, M.I.T. Press, Cambridge, Mass., 1972 (Sections 2.6 and 2.7).

Kinsler, L.E. and Frey, A.R., *Fundamentals of Acoustics*, 2nd Edit., Wiley, New York, 1962 (Section 7.7).

Lindsay, R.B., *Mechanical Radiation*, McGraw-Hill, New York, 1960 (Section 3.5).

Morse, P.M., *Vibration and Sound*, 2nd Edit., McGraw-Hill, New York, 1948 (Section 27).

Morse, P.M. and Ingard, K.U., *Theoretical Acoustics*, McGraw-Hill, New York, 1968 (Section 7.1).

Rayleigh, Lord, *Theory of Sound*, Vol. II, 2nd Edit., London, 1896; Dover, New York, 1945.

Rschevkin, S.N., *Theory of Sound*, Pergamon Press, Oxford, 1963 (Chapter 4).

Section 4.3

Brooke-Benjamin, T., "Surface Effects in Non-Spherical Motions of Small Cavities," in *Cavitation in Real Liquids*, R. Davies (Ed.), Elsevier, Amsterdam, 1964 (pp. 164-180).

Devin, C., Jr., Survey of thermal, radiation and viscous damping of pulsating air bubbles in water, *J.A.S.A.*, *31*, 1654-1667, 1959.

Fitzpatrick, H.M. and Strasberg, M., "Hydrodynamic Sources of Noise," Paper 10 of *Symposium on Naval Hydrodynamics*, Nat. Acad. of Sciences, Nat. Res. Council Publication 515, Washington, D.C., 1956; also *D.T.M.B. Rept. 1269*, 1959.

Gavigan, J.J., Watson, E.E. and King, W.R., III, Noise generation by gas jets in a turbulent wake, *J.A.S.A.*, *56*, 1094-1099, 1974.

Kapustina, O.A., "Gas Bubbles in Liquids," Chapter 1, Part 4 of *Physical Principles of Ultrasonic Technology*, Vol. I, L.D. Rozenberg (Ed.), Plenum Press, New York, 1973 (pp. 382-390).

Lauterborn, W., Resonance frequencies of gas bubbles in liquids, *Acustica*, *20*, 14-20, 1968; *23*, 73-81, 1970 (in German).

Meyer, E. and Tamm, K., Resonant vibrations and damping of gas bubbles in liquids, *Akust. Zeit.*, *4*, 145, 1939; *D.T.M.B. Trans. 109*.

Meyer, E., "Air Bubbles in Water," Chapter 5 of *Technical Aspects of Sound*, Vol. II, E.G. Richardson (Ed.), Elsevier, Amsterdam, 1957.

Minnaert, M., On musical air bubbles and the sounds of running water, *Phil. Mag.*, *16*, 235-248, 1933.

Mühle, C. and Heckl, M., Sound Radiation by Submerged Exhaust, *Müller-BBN Rept. 2605*, 1971, translated from German in *NAVSHIPS Trans. 1321*, 1972.

Shima, A., The Natural Frequency of a Bubble Oscillating in a Viscous Compressible Liquid, *A.S.M.E.* Paper 69-WA/FE-1, 1969.

Shima, A., The natural frequencies of two spherical bubbles oscillating in water, *J. Basic Engin.*, *93*, 426-432, 1971.

Strasberg, M., Pulsation frequency of nonspherical gas bubbles in liquids, *J.A.S.A.*, *25*, 536-537, 1953.

Strasberg, M., Gas bubbles as sources of sound in liquids, *J.A.S.A.*, *28*, 20-26, 1956; also *D.T.M.B. Rept. 1042*, April 1956.

Victor, A.S., A Study of the Damping and Stability of a Pulsating Spherical Bubble in a Flowing Fluid, *U.S.N. Mine Defense Lab. Rept. 329*, April 1967.

Vorotnikova, M.I. and Soloukin, R.I., A calculation of the pulsations of gas bubbles in an incompressible liquid subject to a periodically varying pressure, *Sov. Phys.-Acoustics, 10*, 28-32, 1964.

Section 4.4

Bannister, R.W., Barker, P.H., Browning, D.G. and Denham, R.N., Ambient sea noise measurements near New Zealand, Paper P4 (Abstract), *J.A.S.A., 55*, 418, 1974.

Bardyshev, V.I., Velikanov, A.M. and Gershman, S.G., Experimental studies of underwater noise in the ocean, *Sov. Phys.-Acoustics, 16*, 512-513, 1970; also, *17*, 252-253, 1971.

Bom, N., Effect of rain on underwater noise level, *J.A.S.A., 45*, 150-156, 1969.

Fitzpatrick, H.M. and Strasberg, M., *op. cit.*

Franz, G.J., Splashes as sources of sound in liquids, *J.A.S.A., 31*, 1080-1096, 1959; also *D.T.M.B. Repts. C-595*, Jan. 1955 and *C-627*, July 1955.

Furduev, A.V., Undersurface cavitation as a source of noise in the ocean, *J. Atmospheric and Oceanic Physics, 2*, 523-533, 1966.

Heindsman, T.E., Smith, R.H. and Arneson, A.D., Effect of rain upon underwater noise levels, *J.A.S.A., 27*, 378-379, 1955.

Knudsen, V.O., Alford, R.S. and Emling, J.W., "Survey of Underwater Sound, Report No. 3, Ambient Noise," *Div. 6.1 Nat. Defense Res. Com. Rept. 1848*, 1944.

Knudsen, V.O., Alford, R.S. and Emling, J.W., Underwater ambient noise, *J. Marine Res., 7*, 410-429, 1948.

Perrone, A.J., Ambient noise spectrum level as a function of water depth, *J.A.S.A., 48*, 362-370, 1970.

Piggott, C.L., Ambient sea noise at low frequencies in shallow water of the Scotian Shelf, *J.A.S.A., 36*, 2152-2163, 1964.

Urick, R.J., *Principles of Underwater Sound for Engineers*, McGraw-Hill, New York, 1967 (Chapter 7).

Wenz, G.M., Acoustic ambient noise in the ocean: spectra and sources, *J.A.S.A., 34*, 1936-1956, 1962.

Sections 4.5-4.8

Arndt, L.K., Responses of Arrays of Isotropic Elements in Detection and Tracking, *U.S. Navy Electronics Lab. Rept. 1456*, April 1967.

Bartberger, C.L., *Lecture Notes on Underwater Acoustics*, U.S. Naval Air Development Center, Johnsville, Pa., 1965 (AD 468869) (pp. 163-168, 199-203, 238-260, 272-283, 319-331).

Bobber, R.J., *Underwater Electroacoustic Measurements*, U.S. Govt. Printing Office, Washington, 1970 (Chapter 2).

Carter, A.H. and Williams, A.O., Jr., A new expansion for the velocity potential of a piston source, *J.A.S.A., 23*, 179-184, 1951.

Chetaev, D.N., The effect of subsonic flow velocity on the radiation impedance of a piston in an infinite baffle, *Sov. Phys.-Acoustics, 2*, 319-327, 1956.

Crane, P.H.G., Method for the calculation of the acoustic radiation impedance of unbaffled and partially baffled piston sources, *J. Sound and Vibr., 5*, 257-277, 1967.

Cremer, L., Heckl, M. and Ungar, E.E., *Structure-Borne Sound*, Springer-Verlag, Berlin, 1972 (Section 6.5).

Feit, D. and Duncan, M.E., Numerical evaluation of the radiation impedance for a piston in a nonrigid baffle, *J.A.S.A., 43*, 885-886, 1968.

Greenspon, J.R. and Sherman, C.H., Mutual radiation impedance and near-field pressures for pistons on a cylinder, *J.A.S.A., 36*, 149-153, 1964.

Herrey, E.M.J., Approximate formula for the radiation resistance of a piston set in an infinite wall, *J.A.S.A., 25*, 154-155, 1953.

Horton, C.W., Sr., *Signal Processing of Underwater Acoustic Waves*, U.S. Govt. Printing Office, Washington, 1969 (Chapters 9 and 14).

Hueter, T.F. and Bolt, R.H., *Sonics*, Wiley, New York, 1955 (Chapter 3).

Jones, R.C., Theory of directional patterns of continuous source distributions on a plane, *J.A.S.A., 16*, 147-171, 1945.

Junger, M.C., Surface pressures generated by pistons on large spherical and cylindrical baffles, *J.A.S.A., 41*, 1336-1346, 1967.

Junger, M.C. and Feit, D., *op cit.* (Chapters 3, 5 and 8).

Karnovskii, M.I., Calculations of the radiation resistance of several types of distributed radiator systems, *Sov. Phys.-Acoustics, 2*, 280-293, 1956.

Kinsler, L.E. and Frey, A.R., *op. cit.* (Chapter 7).

Laird, D.T. and Cohen, H., The directivity patterns for acoustic radiation from a source on a rigid cylinder, *J.A.S.A., 24*, 46-49, 1952.

Lindsay, R.B., *op. cit.* (Section 9.10).

Mangulis, V., Pressure on a vibrating circular piston in an infinite baffle, *J.A.S.A., 36*, 1734-1735, 1964.

Molloy, C.T., Calculation of the directivity index for various types of radiators, *J.A.S.A., 20*, 387-405, 1948.

Morse, P.M., *op cit.* (Sections 27 and 28).

Morse, P.M. and Ingard, K.U., *op. cit.* (Chapters 7 and 11).

Rschevkin, S.N., *op. cit.* (Chapter 11).

Schelkunoff, S.A., Mathematical theory of linear array, *Bell System Tech. J., 22*, 80-107, 1943.

Smaryshev, M.D., Radiation impedance and gain of extended periodic linear arrays, *Sov. Phys.-Acoustics, 14*, 499-503, 1968.

Smith, P.W., Jr., Directive Receiving Arrays, *Bolt Beranek and Newman Rept. 913*, March 1962.

Stenzel, H., *Handbook for the Calculation of Sound Propagation Phenomena* (in German), Julius Springer, Berlin, 1939; translated by A.R. Stickley, *NRL Trans. 130*.

Urick, R.J., *op. cit.* (Chapter 3).

Vinogradova, E.L. and Furduev, V.V., Directivity factor of a linear array of directional transmitters, *Sov. Phys.-Acoustics, 12*, 161-163, 1966.

Winder, A.A. and Loda, C.J., *Introduction to Acoustical Space-Time Information Processing*, O.N.R., ACR-63, Washington, Jan. 1963 (Sections E and H).

Young, R.W., Image interference in the presence of refraction, *J.A.S.A., 19*, 1-7, 1947.

Section 4.9

Alfredson, R.J. and Davies, P.O.A.L., The radiation of sound from an engine exhaust, *J. Sound and Vibr., 13*, 389-408, 1970.

Dunham, W.H., "Flow-Induced Cavity Resonances in Viscous Compressible and Imcompressible Fluids," in *Proc. Fourth Symposium on Naval Hydrodynamics*, O.N.R., ACR-92, Washington, 1962 (pp. 1057-1081).

Ffowcs Williams, J.E., "Jet Noise at Very Low and Very High Speed," in *Aerodynamic Noise*, H.S. Ribner (Ed.), Univ. of Toronto Press, 1969 (pp. 131-146).

Harrington, M.C. and Dunham, W.H., Studies of the mechanism for flow-induced cavity resonance, Paper G8 (Abstract), *J.A.S.A., 32*, 921, 1960.

Ingard, K.U. and Dean, L.W., "Excitation of Acoustic Resonators by Flow," in *Proc. Second Symposium on Naval Hydrodynamics*, O.N.R., ACR-38, Washington, 1958 (pp. 137-148).

Krishnamurty, K., Acoustic Radiation from Two-Dimensional Rectangular Cutouts in Aerodynamic Surfaces, *N.A.C.A. Tech. Note 3487*, Aug. 1955.

Morfey, C.L., Acoustic properties of openings at low frequencies, *J. Sound and Vibr., 9*, 357-366, 1969.

Morse, P.M., *op cit.* (Section 23).

Plett, E.G. and Summerfield, M., Jet engine exhaust noise due to rough combustion and nonsteady aerodynamic sources, *J.A.S.A., 56*, 516-522, 1974; *57*, 755, 1975.

Sorokin, V.I., Investigation of water-air reconators, *Sov. Phys.-Acoustics, 4*, 188-195, 1958.

Westervelt, P.J. and McQuillin, R.J., Theory of pulse jet noise generation, Paper D7 (Abstract), *J.A.S.A., 29*, 1252, 1957.

Sections 4.10 and 4.11

Baron, M.L., Bleich, H.H. and Mathews, A.T., Forced vibrations of an elastic circular cylindrical body of finite length submerged in a fluid, *Int. J. of Solids and Structures, 1*, 3-22, 1965.

Bleich, H.H. and Baron, M.L., Free and forced vibrations of an infinitely long cylindrical shell in an infinite acoustic medium, *J. Applied Mech., 21*, 167-184, 1954.

Chen, L.H. and Schweikert, D.G., Sound radiation from an arbitrary body, *J.A.S.A., 35*, 1626-1632, 1963.

Chertock, G., Sound radiation from prolate spheroids, *J.A.S.A., 33*, 871-876, 1961; also *D.T.M.B. Rept. 1516*, Nov. 1961.

Chertock, G., Sound radiation from vibrating surfaces, *J.A.S.A., 36*, 1305-1313, 1964.

Chertock, G., Solutions for sound-radiation problems by integral equations at the critical wave numbers, *J.A.S.A., 47*, 387-388, 1970.

Chertock, G., Integral Equation Methods in Sound Radiation and Scattering from Arbitrary Surfaces, *N.S.R.D.C. Rept. 3538*, June 1971.

Chertock, G., Sound radiated by low-frequency vibrations of slender bodies, *J.A.S.A., 57*, 1007-1016, 1975.

Copley, L.G., Integral equation method for radiation from vibrating bodies, *J.A.S.A., 41*, 807-816, 1967.

Copley, L.G., Fundamental results concerning integral representations in acoustic radiation, *J.A.S.A., 44*, 28-32, 1968.

Donaldson, J.M., Reduction of sound radiated from ship structures, *Applied Acoustics, 1*, 275-291, 1968.

Greenspon, J.E., Theoretical developments in the vibrations of hulls, *J. of Ship Res., 6*, (4)26-46, 1963.

Heckl, M., Vibrations of point-driven cylindrical shells, *J.A.S.A., 34*, 1553-1557, 1962.

Hess, J.L., Solution of the Helmholtz Equation for Steady Acoustic Waves, *Douglas Aircraft Div. Rept. 31655*, April 1964.

Junger, M.C., Vibrations of elastic shells in a fluid medium and the associated radiation of sound, *J. Applied Mech., 19*, 439-445, 1952.

Junger, M.C., Dynamic behavior of reinforced cylindrical shells in a vacuum and in a fluid, *J. Applied Mech., 21*, 35-41, 1954.

Junger, M.C., Radiation and scattering by submerged elastic structures, *J.A.S.A., 57*, 1318-1326, 1975.

Junger, M.C. and Feit, D., *op. cit.* (Chapters 4, 8 and 10).

Kellogg, O.D., *Foundations of Potential Theory*, Dover Publications, New York, 1953 (Chapter 6).

Lamb, Sir Horace, *Hydrodynamics*, 6th Edit., Dover, New York, 1945 (pp. 496-501).

MacNeal, R.H., *Electric Circuit Analogies for Elastic Structures*, Wiley, New York, 1962 (Chapter 8).

McCormick, J.M. and Baron, M.L., Sound radiation from submerged cylindrical shells of finite length, *J. Engin. for Industry, 87B*, 393-405, 1965.

Morse, P.M. and Feshbach, H., *Methods of Mathematical Physics*, Vol. II. McGraw-Hill, New York, 1953.

Murray, M.T., High and low-frequency approaches to the acoustic radiation problem, *J. Sound and Vibr., 34*, 327-356, 1974.

Pond, H.L., Low-frequency sound radiation from slender bodies of revolution, *J.A.S.A., 40*, 711-720, 1966.

Schenck, H.A., Improved integral formulation for acoustic radiation problems, *J.A.S.A., 44*, 41-58, 1968.

Strasberg, M., Radiation from unbaffled bodies of arbitrary shape at low frequencies, *J.A.S.A., 34*, 520-521, 1962.

Tsokos, C.P. and North, E.L., Sound Radiation from a Cylindrical Shell, *Electric Boat Div. Rept. U413-62-173* (and addendum), Dec. 1962 and April 1963 (AD 422496).

Warburton, G., Vibration of a cylindrical shell in an acoustic medium, *J. Mech. Engin. Science, 3*, 69-79, 1961.